# Toward Benchmark-quality Ab Initio Predictions for 3d Transition Metal Electrocatalysts - A Comparison of CCSD(T) and ph-AFQMC

Hagen Neugebauer,[†] Hung T. Vuong,[‡] John L. Weber,[‡] Richard A. Friesner,[‡] James Shee,[*,¶] and Andreas Hansen[*,†]

† *Mulliken Center for Theoretical Chemistry, Clausius Institute for Physical and Theoretical Chemistry, University of Bonn, Beringstr. 4, D-53115 Bonn, Germany*

‡*Department of Chemistry, Columbia University, 3000 Broadway, New York, NY, 10027*

¶*Department of Chemistry, University of California, Berkeley, California 94720, United States*

E-mail: jshee@berkeley.edu; hansen@thch.uni-bonn.de

**Abstract**

Generating accurate *ab initio* ionization energies for transition metal complexes is an important step towards the accurate computational description of their electrocatalytic reactions. Benchmark-quality data is required for testing existing theoretical methods and for developing new ones but is complicated to obtain for many transition metal compounds due to the potential presence of both strong dynamical and static electron correlation. In this regime, it is questionable whether the so-called gold standard, coupled cluster with singles, doubles, and perturbative triples (CCSD(T)), provides the desired level of accuracy – roughly $1-3$ kcal/mol. In this work, we compiled a test set

of 28 3d metal-containing molecules relevant to homogeneous electrocatalysis (termed 3dTMV) and computed their vertical ionization energies (ionization potentials) with CCSD(T) and phaseless auxiliary-field quantum Monte Carlo (ph-AFQMC). A substantial effort has been made to converge away the phaseless bias in the ph-AFQMC reference values. We assess a wide variety of multireference diagnostics, and find that spin-symmetry breaking of the CCSD wavefunction and in the PBE0 density functional correlate well with our analysis of multiconfigurational wavefunctions. We propose quantitative criteria based on symmetry breaking to delineate correlation regimes inside of which appropriately-performed CCSD(T) can produce mean absolute deviations from the ph-AFQMC reference values of roughly 2 kcal/mol or less, and outside of which CCSD(T) is expected to fail. We also present a preliminary assessment of DFT functionals on the 3dTMV set.

# 1 Introduction

Molecular electrocatalysis based on 3d transition metal compounds is an important tool for the synthesis of complex molecules[1,2] and a promising approach for $CO_2$ reduction,[3–6] water splitting,[7,8] oxygen reduction,[9] and other hydrogen evolution reactions[10] employing earth abundant metals.[11] Quantum chemistry (QC) can potentially guide the development of novel catalysts. Elucidating the underlying mechanisms and tuning ligand structures to achieve lower over-potentials, higher turnover frequencies, and better substrate selectivity are typical applications.[12]

However, the choice of a reliable QC method – e.g., density functional theory (DFT) or wave function theory (WFT) – for first-row (3d) transition metal electrocatalysts is more challenging than in the case of organic molecules, as the target systems can be large and often exhibit relatively complicated electronic structures. Transition metal complexes with low coordination number, high symmetry, and/or multiple magnetically-coupled radical sites can have more degenerate or nearly-degenerate orbitals and spin-states, which can result in

multireference (MR) character (also known as static or strong correlation).[13–15] The degree of static correlation increases in many open-shell species or complexes with redox non-innocent ligands that often appear in electrocatalysis.[13,16] Various MR descriptors are available in the literature for detecting such cases with significant static correlation.[17,18] Dynamic correlation effects between multiple electron pairs (for example in carbonyl ligands with $\sigma$-donation and $\pi$-backbonding) can occur as well, which requires a theoretical description beyond second-order perturbation theory.[19,20]

The first step towards robust modeling of experimentally relevant electrocatalysts is the accurate prediction of redox potentials, which besides accurate solvation free energies, requires reliable ionization energies.[21] To test QC methods, multiple benchmarks of transition metal complexes with experimental redox potentials were compiled.[21–26] One shortcoming when employing solely experimental redox potentials as reference is that the electronic structure problem cannot be investigated independently from solvation effects and error compensation hinders the analysis of individual error contributions. Reference ionization energies allow a separation of the error sources from the electronic structure and solvation contributions and enable precise error tracing. For example, this was done in a study by Isegawa *et al.*, who compared experimental ionization and redox potentials of organic compounds to DFT and CCSD(T) calculated potentials.[27] Here, the favorable performance of CCSD(T) for ionization energies diminished for redox potentials due to missing solvation contributions. Sterling *et al.* applied an explicit solvation workflow to include the neglected solvation contributions and obtained excellent agreement with experiment.[28] Another interesting approach that tackles both problems at once is the explicit inclusion of solvent molecules. In a multilayer DLPNO-CCSD(T) study performed by Bhattacharjee *et al.* for first-row transition metals in water,[29] accurate reduction potentials were obtained.

However, only rarely are experimental reference ionization energies available for 3d electrocatalysts; computational protocols that can generate these accurate ionization energies are highly desired. For main group chemistry, benchmark-quality reference ionization po-

tentials and electron affinities can be generated with CCSD(T)[30] as done for medium-sized acceptor molecules by Richard *et al.*[31] Because of the varying (and sometimes large) degree of static correlation encountered in 3d transition metal electrocatalysis, the expected accuracy of CCSD(T) is unclear. For transition metal atoms CCSD(T) can yield accurate results for ionization energies,[32] but for many diatomic molecular bond dissociation energies the predictive power of CCSD(T) deteriorates.[33–38] However, for experimentally derived spin splittings of non-heme iron complexes as well as metallocenes, CCSD(T), especially when based on Kohn-Sham (KS) orbitals, yielded accurate results.[39,40] Good performance for CCSD(T) with KS orbitals could also be observed for calculating vibrational frequencies.[41] Another issue is that molecules of medium to large size cannot be treated by canonical CCSD(T). This is especially the case at the complete basis set (CBS) limit, which is required for benchmark-quality data to be comparable to experimental measurements. Therefore, less expensive but also potentially less accurate localized coupled cluster schemes are often employed. One of the most prominent of these schemes is DLPNO-CCSD(T).[42–44] For reactions involving singlereference (SR), large-gap states, DLPNO-CCSD(T) can be employed as a reliable reference method for benchmarking closed-shell (MOR41)[45] and open-shell (ROST61)[46] organometallic reactions. The efficiency of the DLPNO-CCSD(T) model has been demonstrated via applications to very large systems, including metalloenzymes.[47] Iron *et al.* used the method to compute transition metal barrier heights in the MOBH35 study.[48,49] Later, a revision to their DLPNO-CCSD(T) references was suggested on the grounds of static correlation effects,[50] but a study by Altun *et al.* traced the DLPNO error to correlation effects from the 3s and 3p semi-core orbitals and to dynamical correlation-induced orbital relaxation effects.[51] In another study the DLPNO approach performed well for challenging spin-splitting energies of iron complexes and reproduced CASPT2/CC results with a two-point PNO extrapolation and improved full iterative triples.[52] Results of similar quality were found for the ionization energy of cobaltocene.[53]

Nevertheless, it would be highly desirable to use accurate and scalable methods to cross-

check CCSD(T) and its localized schemes. A promising candidate for this task is the phaseless auxiliary field quantum Monte Carlo (ph-AFQMC) method,[32,54–57] which was originally developed in the physics community.[58,59] Recently, a localized orbital version (LO-ph-AFQMC) has been developed.[60] Especially relevant for transition metal chemistry is the nonperturbative and inherently MR nature of this method. In principle, the phaseless bias can be converged away by systematically improving the trial wavefunction toward the exact wavefunction. Once a trial wavefunction is obtained, the cubic scaling computational cost with system size and near-perfect parallel efficiency of LO-ph-AFQMC enables applications to relatively large molecular systems, at least when compact trail wavefunctions are required. However, due to the stochastic nature of the method, one must typically sample thousands of trajectories to obtain adequate statistics. Encouragingly, the scaling prefactor has been reduced significantly via efficient implementations on graphical processing units (GPUs),[32,61] and the branching random walks are amenable to massively parallel computing systems that can efficiently utilize hundreds of GPUs at a time. ph-AFQMC has been successfully used to calculate accurate ionization potentials for transition metal atoms,[32] dissociation energies of transition metal containing diatomics,[37] ligand dissociation energies[62] and ionization potentials[63] of transition metal complexes. Alternative accurate MR methods include the recently developed CASPT2+$\delta$MRCI approach for spin-splittings,[64,65] but this approach is not feasible for the system sizes at hand.

In this work, we compile a set of medium-sized 3d transition metal complexes relevant to electrocatalysis. We compare CCSD(T) and ph-AFQMC predictions, and investigate the degree of MR character present using a variety of diagnostics. We propose a quantitative classification protocol, involving the dominant coefficient in multiconfigurational wavefunctions and the degree of spin-symmetry breaking or restoration from coupled cluster wavefunctions and from the PBE0 density functional, to gauge the expected accuracy of various coupled cluster approaches. For vertical ionizations involving predominately SR systems, average errors of less than 2.3 kcal/mol can be achieved with a specific choice of orbitals and

spin restriction. In contrast, large deviations between all CCSD(T) protocols and reference ph-AFQMC values were observed for ionizations involving states exhibiting strong static correlation. In contrast to other studies in which many coupled cluster approaches were tested for a specific, smaller system,[66] we investigate only select CC protocols for which i) the required computational demands exceed those of CCSD(T) by at most a factor of two, and ii) local implementations are available for subsequent studies with extended basis sets.

## 1.1 Design of the 3dTMV Benchmark set

The 3dTMV benchmark was generated with the following design criteria in mind. We chose complexes which (i) have experimental relevance to electrocatalysis (e.g. hydrogen evolution, $CO_2$ reduction), (ii) are of medium size (20-40 atoms), and (iii) contain one or two transition metal atoms. The molecules included in the 3dTMV set are depicted in Figure 1. Their charges, multiplicities, and experimental references are given in Table 1. The vertical ionization energies, which we will refer to in the following as ionization potentials (IPs), were calculated. The calculation of vertical ionization energies is more challenging than for adiabatic ionization potentials because the oxidized species are not in their optimal ground state geometry, which can lead to more challenging electronic structures. The classification of the IPs into SR, SR/MR, and MR subsets is discussed in detail in Section 3.2.

Complexes **1** and **2** are two of the few studied complexes for fuel generation with titanium.[67,68] Complexes **3-5**, **13**, and **14** are all metallocenes of which ferrocene is of special interest to electrochemistry due to its ideal reversible oxidation.[69–73] The IPs have already been investigated in Ref. 63, and there is renewed interest in the isolation and electronic structures of the manganocene, ferrocene and cobaltocene anions.[74,75] Systems **6**, **7**, and **19** are examples of iron-based three-legged piano-stool catalysts[76–79] and **8-10** are models of three-legged piano-stool catalysts with cobalt.[80] System **11** is a cyclam model,[81] while **12** is a model for the DuBois type catalyst.[82] The carbonyl bipyridine complexes **15-18** are model catalysts for more elaborate pyridine based catalysts.[83–86] The cobalt complexes **20** and **23**

are examples of cobaloximes that have been employed for $H_2$ generation.[87–90] System **21** is a nitrogen reduction catalyst that can reduce dinitrogen into ammonia and hydrazine.[91] Complex **22** is a cutout from a hydrogenase model.[92] The chromium complex **24** and the iron complex **25** are acetylacetone (acac) complexes that are widely studied as models for other tris-$\beta$ diketonate complexes and have also been investigated in Ref. 63. $Fe(acac)_3$ is also of interest for photoredox catalysis.[93] Complex **26** is a hydrogenase mimic[94] and the only system with two metal atoms in the set. The planar complexes **27** and **28**, relevant for hydrogen generation,[95,96] are especially challenging due to their redox-active ligands.[97]

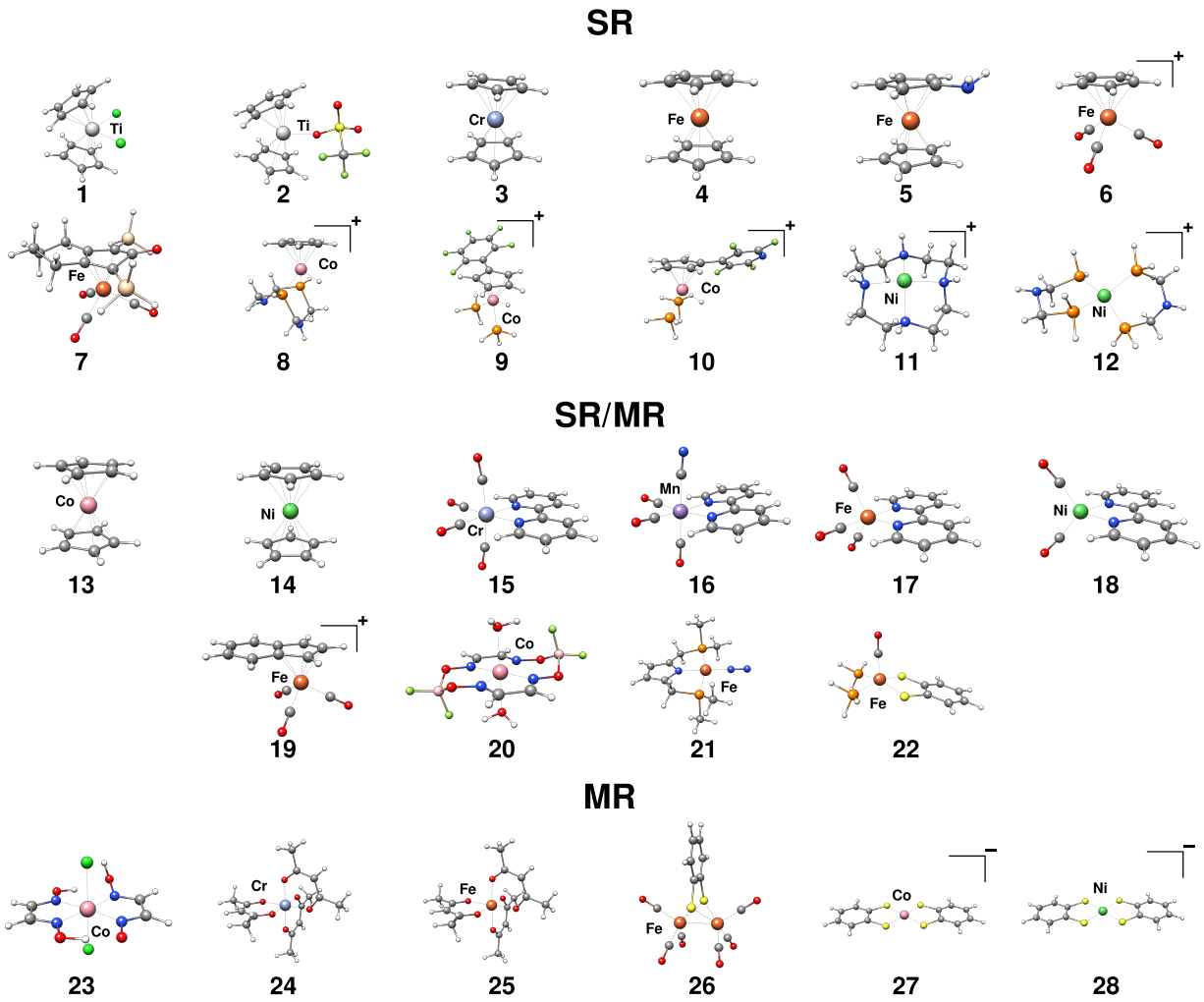


Figure 1: Structures included in the 3dTMV benchmark set divided into singlereference (**SR**), an intermediate category (**SR**/**MR**), and multireference (**MR**) subsets.

Table 1: Molecules included in the 3dTMV set with corresponding charges and spin multiplicities for the oxidized (ox) and initial (in) state as well as experimental studies where these complexes were investigated.

| # | charge | | multiplicity | | Ref. | # | charge | | multiplicity | | Ref. |
|---|---|---|---|---|---|---|---|---|---|---|---|
| | ox | in | ox | in | | | ox | in | ox | in | |
| 1 | 1 | 0 | 2 | 1 | [ 67] | 15 | 1 | 0 | 2 | 1 | [ 83] |
| 2 | 1 | 0 | 1 | 2 | [ 68] | 16 | 1 | 0 | 2 | 1 | [ 84] |
| 3 | 1 | 0 | 4 | 3 | [ 98] | 17 | 1 | 0 | 2 | 1 | [ 85] |
| 4 | 1 | 0 | 2 | 1 | [ 70] | 18 | 1 | 0 | 2 | 1 | [ 86] |
| 5 | 1 | 0 | 2 | 1 | [ 73] | 19 | 2 | 1 | 2 | 1 | [ 77] |
| 6 | 2 | 1 | 2 | 1 | [ 76] | 20 | 1 | 0 | 3 | 2 | [ 87] |
| 7 | 1 | 0 | 2 | 1 | [ 78] | 21 | 1 | 0 | 3 | 2 | [ 91] |
| 8 | 2 | 1 | 2 | 1 | [ 80] | 22 | 1 | 0 | 2 | 1 | [ 92] |
| 9 | 2 | 1 | 2 | 1 | [ 80] | 23 | 1 | 0 | 2 | 1 | [ 88] |
| 10 | 2 | 1 | 2 | 1 | [ 80] | 24 | 1 | 0 | 3 | 4 | [ 99] |
| 11 | 2 | 1 | 1 | 2 | [ 81] | 25 | 1 | 0 | 3 | 6 | [ 99] |
| 12 | 2 | 1 | 1 | 2 | [ 82] | 26 | 1 | 0 | 2 | 1 | [ 94] |
| 13 | 1 | 0 | 1 | 2 | [ 98] | 27 | 0 | -1 | 2 | 3 | [ 95] |
| 14 | 1 | 0 | 2 | 3 | [ 98] | 28 | 0 | -1 | 1 | 2 | [ 96] |

# 2 Computational Methods

## 2.1 DFT and Coupled Cluster Calculations

Geometries were optimized with the r$^2$SCAN-3c level of theory[100] in TURBOMOLE 7.5.1.[101,102] All singlepoint DFT calculations, if not stated otherwise, were performed with the double-$\zeta$ def2-SVP basis set[103] in ORCA 5.0.3[104] employing the *DEFGRID3* and the *TightSCF* settings. Namely, the GGA functional PBE,[105,106] the meta-GGA functionals r$^2$SCAN[107,108] and M06-L,[109] the hybrid functionals PBE0,[110] r$^2$SCAN0,[111] B3LYP,[112,113] PW6B95,[114] and M06-2X[115] as well as the range separated hybrid $\omega$B97X-V,[116] and the double hybrid PWPB95[117] were used. Robust SCF convergence for DFT calculations was ensured by employing the TRAH SCF solver.[118] The split-RI-J approximation was used to speed up DFT calculations[119] using the corresponding auxiliary basis set[120] and hybrid DFT calculations were additionally sped up with the RIJCOSX approximation.[121–123] To account for

London Dispersion effects the D4 dispersion correction[124] was employed in the dftd4 v.3.4.0 standalone program.[125] The local-hybrid LH20t DFT functional[126] was employed in TURBOMOLE 7.5.1. and the hybrid KP16 functional[127] was employed in the xTron program package.[128] CCSD(T) calculations were performed in the Q-Chem 5.4 program package[129] with the cutoff for neglecting two electron integrals set to $10^{-14}$ and the SCF convergence set to $10^{-8}$. To ensure robust SCF convergence, the GDM algorithm was employed as SCF solver[130] and the internal stability analysis was used to verify SCF solutions as minima in orbital space. The LIBPT library was used for evaluation of the triples contribution. DFT calculations for follow up CCSD(T) calculations in Q-Chem were performed with the PBE0 functional[110] and the SG-1 grid.[131] To account for correlation effects in the 3s and 3p shells of 3d transition metals, the frozen core settings in the correlated calculations were adjusted to only freeze the 1s, 2s, and 2p shells of 3d transition metal atoms. The importance of these core-valence correlation contributions has been emphasized recently for 3d transition metals in the context of DLPNO-CCSD(T)[51] and CASSCF[132] calculations.

In the following UHF/RHF means that singlets were calculated with restricted Hartree-Fock (RHF) and all other spin multiplicities with unrestricted Hartree-Fock (UHF). Similarly, orbital protocols such as RPBE0/UPBE0 indicate that R and U are used for singlets and non-singlets, respectively. The ROHF/RHF CR-CC(2,3)[133,134] calculations were performed with a serial implementation from GAMESS 2021 R2 Patch 2.[135,136]

## 2.2 ph-AFQMC Calculations

### 2.2.1 Trial wavefunctions and the phaseless bias in AFQMC

In principle, it should be possible to systematically converge AFQMC calculations, even for strongly MR transition metal containing species, by systematically increasing the quality of the trial wavefunction until a stable value of the observable (in this case the ionization potential of the complex) is obtained. In practice, the question of how to best optimize a multideterminental wavefunction for AFQMC for transition metal containing systems is at

present a challenging basic research problem. In the present paper, we utilize two different approaches based on the degree of MR character, which will be outlined below. While we do not claim to have a universally valid, rigorously converged protocol (which would require studying substantially larger and more diverse datasets, as well as a considerably larger investment of computational resources), we do believe that the results reported here represent progress in controlling the error in the calculations for these challenging cases as compared to our prior efforts. The significant fluctuations in the CCSD(T) results, seen even in the test cases judged to be squarely in the SR regime, are indicative of the difficulty of obtaining ionization potentials that are robustly of chemical accuracy.

Our initial work using AFQMC methods to study transition metal containing species investigated three types of trial functions: Hartree Fock (both restricted and unrestricted), DFT (primarily unrestricted), and CASSCF. For difficult cases, CASSCF trials were generally required, although computational limitations significantly restricted the size of the active space that could be employed. The lack of scalability of CASSCF (with regard to both active space dimension and overall molecular size) motivated us to explore the use of selected CI approaches, which enable the investigation of substantially larger active spaces than what is accessible through CASSCF. The trial wavefunctions used for the SR and SR/MR subsets were from a variational selected CI procedure, which we refer to as HCISCF.[137,138] Configurations were selected using $\epsilon_1 = 10^{-4}$ a.u. Active spaces were chosen as follows: First, the eigenvalues (orbital energies) of the Fock or Kohn-Sham operator are obtained, and the sequential energy differences were plotted. We made cuts between orbitals that have relatively large energetic separation, such that $24 - 43$ active orbitals are kept in a subsequent optimization of both selected CI coefficients and orbital coefficients. Between 88 and 92 percent of the HCISCF CI weight was retained in the ph-AFQMC trial wavefunctions, which corresponds to between 5 and 1199 determinants (a relatively small number compared to the full Hilbert space). In some cases (see the SI), B3LYP orbitals were used as an initial guess for the HCISCF optimization. This was done when a lower-energy solution at the HCISCF

level could be obtained, when the initial HCISCF calculations using HF orbitals as a starting point did not converge, or when the HF orbitals were found to be qualitatively wrong (*vide infra*).

In order to get a sense of the sensitivity of our results for the SR and SR/MR subsets to the trial wavefunction employed, we also experimented with two alternative protocols which will be presented in a future work. In the first, a CASSCF optimization in a small active space is followed by a single-shot selected CI calculation in a larger active space. In the second, we use an initial selected CI calculation in a very large active space (with a relatively loose selection threshold) and use natural orbital occupation number cutoffs to define a smaller active space which can be treated with a tighter cutoff. We find mean absolute deviations from the present predictions with HCISCF trials of roughly 1.4 and 2.1 kcal/mol, which are a little larger than what would traditionally be considered "chemical accuracy" (1 kcal/mol) but well within the looser criterion of "transition metal chemical accuracy" (1-3 kcal/mol),[33] which we believe is an appropriate target for the current state of the art in electronic structure technology for these systems, and which is capable of providing a very reasonable picture of reaction thermochemistry for complex problems in materials and biology. To conservatively account for any residual error due to the possibility of unconverged phaseless bias in the SR and SR/MR subsets, we report (in the Figures to follow) a total uncertainty on the predicted IPs which represents the statistical error of each energy difference plus 1.5 kcal/mol for the SR and SR/MR subsets.

For the MR set, we attempted to converge our ph-AFQMC predictions with respect to three different dimensions: the size of the active space, the value of $\epsilon_1$ in selected CI, and the % CI weight retained in the trial wavefunction (which we abbreviate hereafter as % CI). Regarding active spaces, three different active space sizes were chosen: a small space of $\leq 18$ orbitals, a medium-sized space with typically 40 to 50 orbitals, and a large-sized active space with some $60 - 80$ orbitals. These active spaces were selected by making cuts based on the orbital energies obtained from a PBE0 calculation, similar to the SR and SR/MR subsets.

We generated a CASSCF trial for the smallest active space, using PBE0 orbitals as starting point, then assessed qualitatively the MR character using the natural orbital occupation numbers (NOONs) and the $1 - C_0^2$ values. The medium and large active space trials were then generated from HCI (no SCF) calculations using the orbitals optimized from CASSCF. Three different choices of $\epsilon_1$ were investigated: $10^{-3}$, $10^{-4}$, and $5 \times 10^{-5}$ a.u. We note that in every case except complex **23** the ph-AFQMC IPs with $\epsilon_1$ of $10^{-4}$ and $5 \times 10^{-5}$, which represents the addition of 294-581 determinants, are converged to within statistical error bars (the difference in the IP is 4.6 ± 1.6 kcal/mol for **23**, which will be discussed further below). Finally, ph-AFQMC calculations were performed with at least three different %CI in the largest active space with $\epsilon_1 = 5 \times 10^{-5}$ trials. All MR trials for ph-AFQMC were in the natural orbital (NO) basis. Additional details, energies and ionization potentials are given in the Supporting Information.

All ph-AFQMC calculations utilized a population control (PC) scheme, in which walkers with large overlaps with the trials are duplicated while those with small weights are purged periodically. However, the above three-dimensional convergence could not be unambiguously shown for complex **25**. In this case, keeping 89, 91, and 93% of the CI weight in the trial wavefunctions produced ph-AFQMC IPs of 225.6 ± 1.3, 224.8 ± 1.1, and 221.4 ± 1.1 (see Table S22). Keeping higher %CI in the trials is currently too computationally demanding with our current implementation, in an active space of 70 electrons in 78 orbitals with $\epsilon_1 = 5 \times 10^{-5}$ a.u. Therefore, we used a correlated sampling (CS) approach in this case, which produced an IP of 215.8 ±1.3 kcal/mol. Interestingly, this value is not far from what one would obtain from extrapolating the three PC results above to the 100% CI weight limit. Indeed, CS has been shown to produce results that are less sensitive to the trial wavefunction employed (and thus closer to the exact, unconstrained result).[54] This method has previously been shown to yield agreement with exact/experimental values for vertical ionization potentials of metallocenes;[63] in difficult cases, CS ph-AFQMC has yielded superior results vs the PC approach for a fixed trial wavefunction. However, we did not use CS for the

entire 3dTMV set because without the removal of walkers with small or vanishing weights it can be more expensive than the PC ph-AFQMC algorithm, and we preferred the ability to check total energies, and their convergence for MR systems.

Taken together, while we have made our best effort to produce accurate reference values with ph-AFQMC, we cannot claim to have achieved exact IPs especially for the cases in the MR subset. For the MR subset we report a total uncertainty which is the statistical error plus 3 kcal/mol. We think this is a reasonable estimate given that other possible error metrics, e.g. the difference in IPs with $\epsilon_1$ of $10^{-4}$ vs $5 \times 10^{-5}$, suggest an average difference of less than 1.5 kcal/mol. While most of the IPs appear to be converged with respect to the trial wavefunction, as can be seen in the SI, some of the cases are strikingly sensitive to the quality of the trial wavefunction. For instance, for complex **23** the ph-AFQMC IP goes from 209.6 to 209.8 to 204.7 kcal/mol in small, medium, and large active space sizes, and in the latter size the IP is 204.7, 203.2, 200.1, and 198.9 kcal/mol with 85, 87, 89, and 90 %CI (all these IPs have associated statistical error bars in the range of 1-1.2 kcal/mol). Admittedly, the added uncertainty of 3 kcal/mol for the MR cases was chosen somewhat arbitrarily. But we note that the level of accuracy that we target is "transition metal chemistry accuracy" and that the spread of the various CC approaches for complex **23** easily exceeds 20 kcal/mol.

### 2.2.2 Computational Details of the ph-AFQMC Calculations

All electrons were correlated in the ph-AFQMC calculations. Electron repulsion integrals and the trial wavefunctions were generated with PySCF.[139] We utilized a localized orbital implementation of ph-AFQMC[60] with a threshold of $5 \times 10^{-5}$ a.u., in which occupied orbitals outside of the active space are localized, and the half-rotated Cholesky matrices are "compressed" using singular value decomposition.[60] Typical compression rates for the systems in the set were $60 - 80\%$. ph-AFQMC calculations used a mixed-precision scheme, wherein floating point operations carrying out the imaginary-time propagation were performed with double-precision while two-electron integrals are stored in single-precision. Test calculations

are shown for complex **1** in the SI, which show that the Cholesky and localization thresholds along with the use of our approximate mixed-precision scheme have negligible effects on the reported ionization energies, given the statistical error bars.

## 2.3 Multireference Diagnostics

Multiple proposed diagnostics for static correlation have been considered, and are detailed in the SI. The principal component analysis of the MR diagnostics was performed in the R statistical environment[140] (version 4.2.0).

For practical purposes, one can distinguish between diagnostics obtained from relatively cheap HF or DFT calculations and diagnostics obtained from higher-scaling correlated WFT methods. While, e.g., CCSD calculations, which formally scale with the 6th power of the system size in most canonical implementations, can often be performed for small to medium-sized molecules in a minimal or double-zeta basis set, in our experience, for systems with >50 atoms, even this is not computationally feasible. In this regime, not to mention when predictions must be extrapolated to the CBS limit, MR diagnostics which use SCF-level information are often the only option.

The HF- and DFT-based diagnostics include the deviation of the total spin expectation value of UHF or a determinant made from UPBE0 orbitals from the exact value:

$$\Delta\langle S^2\rangle = \langle S^2\rangle_{\text{method}} - \langle S^2\rangle_{\text{exact}}. \tag{1}$$

Spin-symmetry breaking (SSB) in approximate electronic structure theories which incorporate some degree of dynamic correlation has been put forth as a diagnostic of static correlation, since it encodes the physical effects (as can be seen in open-shell singlets) when low-lying excited states of higher multiplicity approach near-degeneracy and mix into a SR

wavefunction.[13,20,141] In this work, we use a regularized percentage quantity:

$$\text{reg. } \Delta\langle S^2\rangle = \frac{100 \cdot |\Delta\langle S^2\rangle|}{MAX(\langle S^2\rangle_{\text{exact}}, 0.75)}. \tag{2}$$

where the regularization parameter of 0.75 was selected to weight the spin contamination in singlets equivalently as in doublets. The number of SCF iterations required to achieve convergence is also considered. The fractional occupation density (FOD)[142] was employed with the r$^2$SCAN[107,108] and the hybrid r$^2$SCAN50[111] functionals. In the FOD formalism, finite-temperature DFT is employed to enable fractional orbital occupations yielding the $N_{FOD}$ value upon integration of their respective density. Because the $N_{FOD}$ value is not size-consistent, the fractional occupation numbers (FON) from FOD calculations were expressed as Matitio's nondynamical correlation index,[143,144] which is a size-consistent form suggested by Martin *et al.* ($r_{nd}$(r$^2$SCAN/r$^2$SCAN50)).[145]

With regard to diagnostics from correlated WFT methods, the well-known $T_1$ diagnostic,[146] the number of required iterations for the coupled-cluster amplitudes (#CC) and the spin contamination at the CCSD level were considered, with UHF and UKS reference determinants. Also, the leading coefficients of the trials (specified in the Supporting Information) in the NO basis for the ph-AFQMC calculations were also employed as static correlation indicator ($1 - C_0^2$).

# 3 Results

## 3.1 Analysis of Multireference Diagnostics

We perform a statistical analysis of the myriad MR diagnostics mentioned above, in an effort to correlated their predictions regarding the presence of static correlation, which will guide our classification of the 3dTMV complexes into subsets. In order to cluster the different diagnostics, a principal component analysis of the pearson correlation matrix (visualized in

Figure 2a) was performed and diagnostics were clustered according to their contribution to principal components as shown in Figure 2b. The first two principal components account for 73.3 % of the variance and were used to cluster the variables. Cluster 1 contains the WFT based diagnostics $\Delta\langle S^2\rangle_{\mathrm{CCSD}}$, $1-C_0^2$, and the $\Delta\langle S^2\rangle_{\mathrm{PBE0}}$. Cluster 2 only contains $\Delta\langle S^2\rangle_{\mathrm{UHF}}$. Cluster 3 contains the number of SCF iterations with HF and PBE0, the $\mathrm{T}_1$(HF) diagnostic, the number of CC iterations for a HF reference, and the finite-temperature DFT based diagnostics ($\mathrm{r_{ND}}$). Cluster 4 contains the $\mathrm{T}_1$ diagnostic and the number of CC iterations with PBE0 reference orbitals.

In cluster 1, $1-C_0^2$ is directly related to the definition of MR character, in the sense that it indicates when more than one configuration has a large weight in the wavefunction. The $\Delta\langle S^2\rangle$ diagnostics in this cluster, which are computed from CCSD wavefunctions or PBE0 orbitals, have been demonstrated to reveal "essential" spin-symmetry breaking, i.e., the spin-contamination in theories which include dynamical correlation provides a better physical description of the static correlation. $\Delta\langle S^2\rangle_{\mathrm{UHF}}$ is not part of this cluster, as one might expect, because HF (which does not formally include any Coulomb correlation) artificially stabilizes high spin states relative to low-spin states, and thus its spin-symmetry breaking behavior is not a reliable indicator of MR character.

The relatively good correlation between the $\mathrm{T}_1$ diagnostic and the number of CC iterations in Cluster 3 and 4 can be interpreted in the following way: Both indicate that CCSD requires many orbital rotations to remedy shortcomings in the reference wavefunction. We emphasize that large values do not necessarily indicate MR character but rather that the reference wavefunction is inadequate. Similar observations regarding the $\mathrm{T}_1$ diagnostic have also been made by others.[17,36]

To obtain a subset of $k$ principal variables that span a space similar to the variables in cluster 1, the variables included in this cluster were further analysed with the "subselect" module developed by Cadima et al.[147] Within the module the "eleaps" algorithm with the GCD (generalized coefficient of determination) as the objective function was selected. The

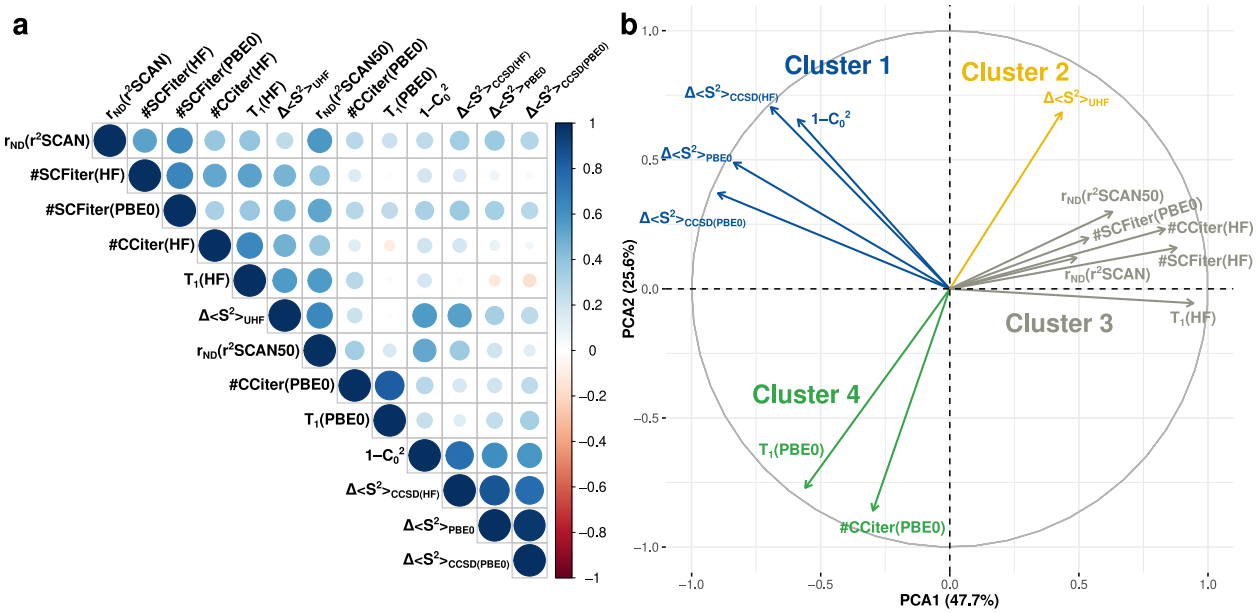


Figure 2: (**a**) Visualized correlation matrix for the static correlation diagnostics. (**b**) Plot of the first two principle components (clusters are indicated by color).

following subsets of increasing size were obtained:

$k = 1$: $\Delta\langle S^2\rangle_{\text{PBE0}}$, GCD=91.4%

$k = 2$: $(1 - C_0^2) + \Delta\langle S\rangle^2_{\text{CCSD(PBE0)}}$, GCD=97.5%

$k = 3$: $(1 - C_0^2) + \Delta\langle S\rangle^2_{\text{CCSD(HF)}} + \Delta\langle S\rangle^2_{\text{CCSD(PBE0)}}$, GCD=99.6%

The large GCD of 91.4% for $k = 1$ with $\Delta\langle S^2\rangle_{\text{PBE0}}$ demonstrates that cluster 1 can be represented well by $\langle S^2\rangle_{\text{PBE0}}$ alone. This empirically validates the usefulness of $\langle S^2\rangle_{\text{PBE0}}$, especially since it is the variable of cluster 1 that is obtained with the least computational effort.

## 3.2 Classification into Subsets

Cluster 1 was employed to partition the 3dTMV IPs into subsets as depicted in Figure 3. We note that although $1 - C_0^2$ reports directly on how dominant the configuration of largest weight is in the linear superposition (and thus is the most physically transparent quantity), the values depend on the choice of active space and may be biased due to missing dynamical correlation effects. On the other hand, while physically justifiable, the degree of

spin-symmetry breaking depends on the degree of inclusion of dynamical correlation (e.g. exhibits xc functional dependence) and in the CC context is derived from a perturbative analysis.[148] Therefore, in what follows, our classification will incorporate four quantities: $1-C_0^2$ and spin-symmetry breaking or restoration from CC/UHF, CC/UPBE0, and UPBE0.

The partitioning was performed with the following criteria and the IP was assigned if either the initial or the oxidized state fulfilled them. IPs where neither the initial nor the oxidized species exceed a deviation for the regularized $\langle S^2 \rangle$ value of 5% and a $1 - C_0^2$ value of 0.28 were put in SR subset. Cases where only one or two of the regularized $\langle S^2 \rangle$ values exceeds the 5% deviation threshold and $1-C_0^2$ is still below 0.28 were put in an intermediate category, which we denote SR/MR. If all three $\langle S^2 \rangle$ diagnostics (in cluster 1) exceed the 5% deviation threshold, and $1 - C_0^2$ is above 0.28, the IP was assigned to the MR subset. There are some exceptions to the threshold based classification. For the complexes **11** and **12** the oxidized species exhibit large $\langle S^2 \rangle$ deviations but only small $1 - C_0^2$ values. At the SCF level the triplet state is predicted to be the ground state, resulting in what has been referred to as "variational collapse"[13] when targeting the singlet state (see SI section 4.4 for details). Subsequent CCSD calculations on these SCF solutions are not able to completely restore the SSB introduced. The large $\langle S^2 \rangle$ deviations for these complexes therefore do not indicate MR character and the corresponding IPs are sorted into the SR subset. Separately, complex **14** is a borderline case and was sorted into the SR/MR subset.

The values of the four diagnostics in cluster 1 are shown in Figure 3 for the IPs classified into SR, SR/MR, and MR subsets. While nearly all of the complexes broke spin symmetry at the UHF level (see Table S2 in the SI), this symmetry breaking is artificial, certainly in the SR subset. In the SR/MR subset, in almost all cases the SSB from CC/UHF is significantly reduced with CC/UPBE0, and UPBE0. In other words, there is a set of non-HF orbitals which reduces the spin-contamination in the reference, which typically enables substantial spin symmetry restoration in the CCSD/UPBE0 wavefunction. It is noticeable that in almost all cases except **17** and **21**, one state, typically the oxidized one, shows significantly larger

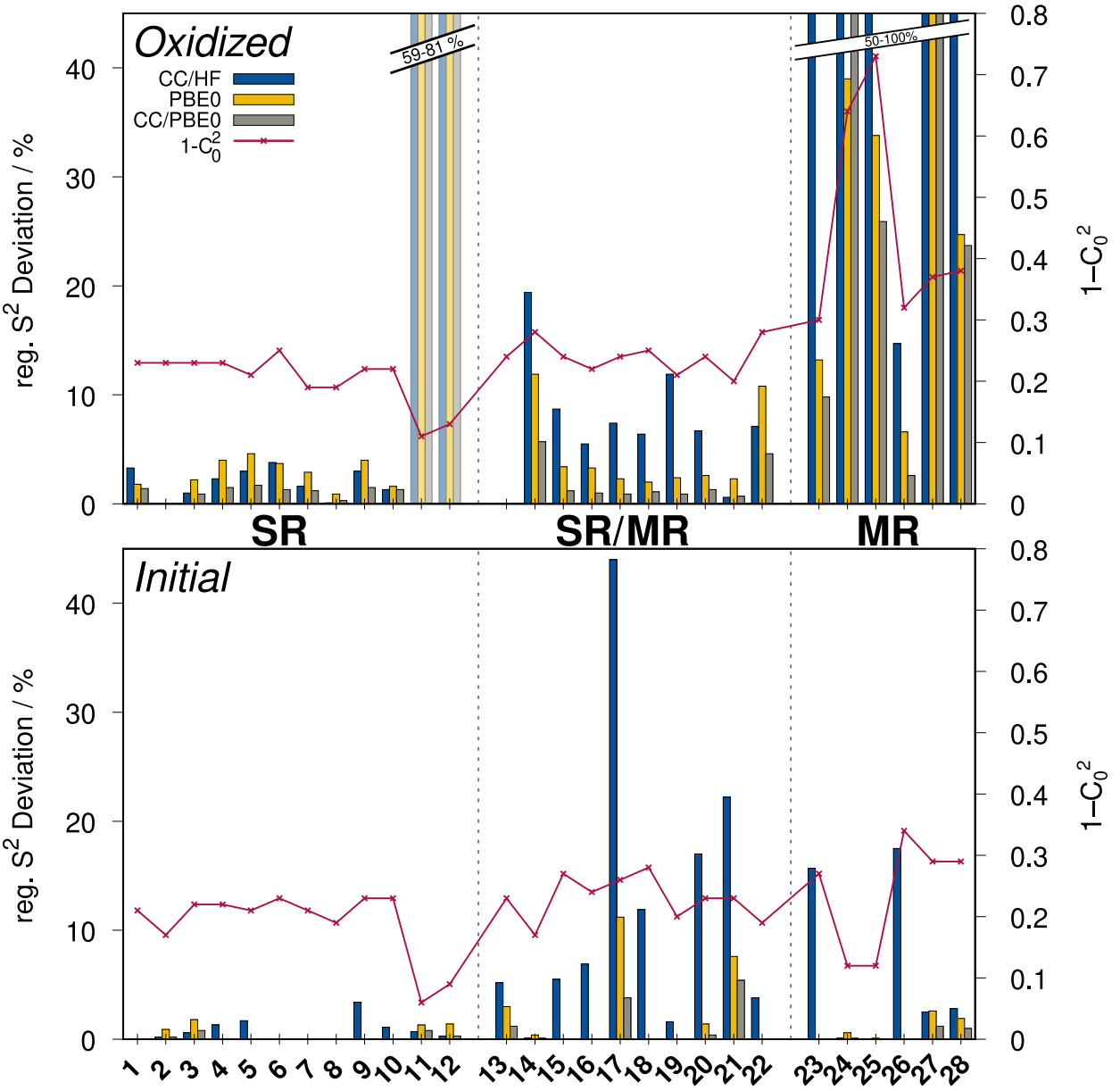


Figure 3: Values of the cluster 1 diagnostics for species in the 3dTMV set. Oxidized species are shown at the top and initial species at the bottom. The left vertical axis shows the regularized $\langle S^2 \rangle$ deviations quantified as a percentage, i.e. $(|\langle S^2 \rangle - \langle S^2_{\text{exact}} \rangle|) * 100/MAX(\langle S^2 \rangle_{\text{exact}}, 0.75)$. $C_0$ values are from the multiconfigurational trial wavefunctions used in ph-AFQMC, as specified in the SI.

SSB than the other, which motivated us to test EOM-IP-CC methods. Finally, the MR subset on average shows large SSB behavior vs the other two subsets. In many cases the $1 - C_0^2$ value is significantly above 0.28, in the range of $0.6 - 0.7$ for the oxidized states of the Cr- and Fe-centered acac complexes.

### 3.3 Comparison of CCSD(T) and LO-ph-AFQMC

Figure 4 compares the deviation in the IPs calculated by three flavors of CCSD(T) vs. the reference ph-AFQMC values. Statistics for each of the three subsets are shown in Table 2.

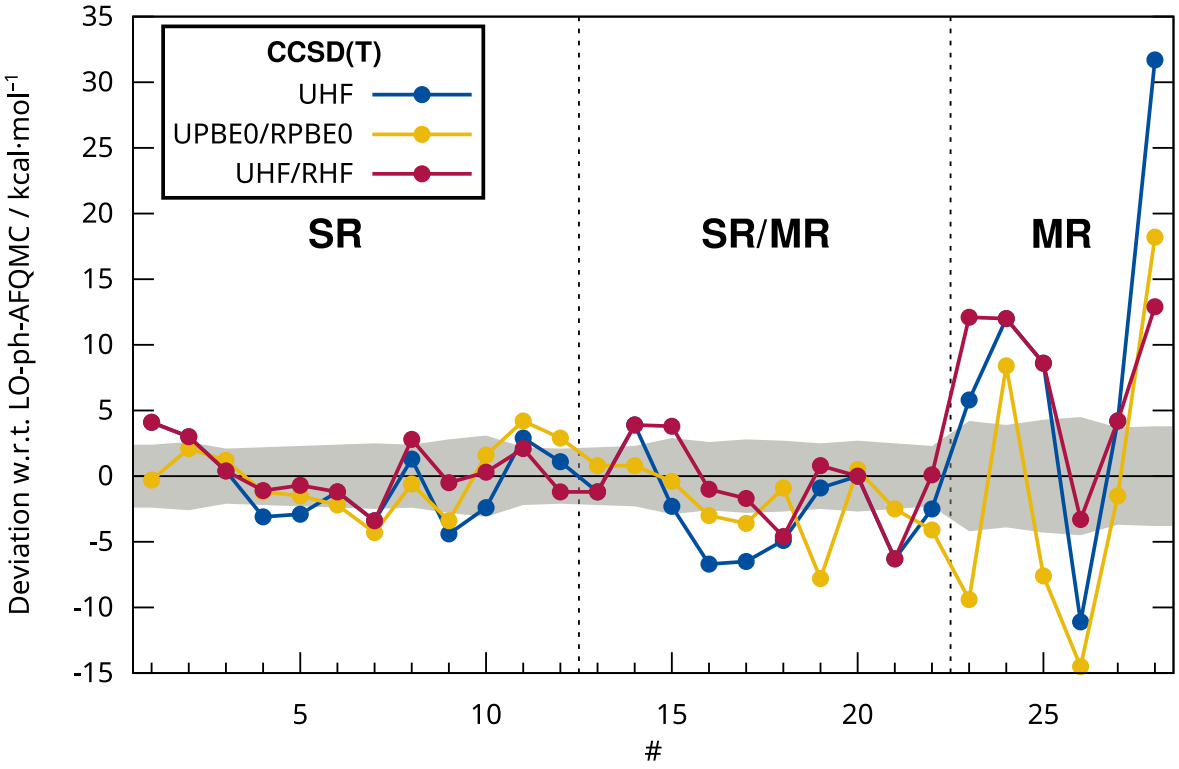


Figure 4: Comparison of CCSD(T) with different orbitals with respect to LO-ph-AFQMC. All IPs are given in the SI in Table S8. The mean IP with LO-ph-AFQMC is 179.2 kcal/mol. Dots are connected by lines to guide the eye.

Table 2: Statistical comparison between CCSD(T) with UHF, UPBE0, UHF/RHF, and ROHF/RHF orbitals (see section 2.1 for details) with respect to LO-ph-AFQMC. The statistical quantities are mean deviation (MD), mean absolute deviation (MAD), standard deviation (SD), and absolute maximum deviations (AMAX), defined in the SI. Statistical evaluation with ROHF/RHF orbitals over the whole set without **24** and **25** from the MR set are given in parenthesis.

| Set | CCSD(T) | MD | MAD | SD | AMAX |
|---|---|---|---|---|---|
| SR | UHF | −0.4 | 2.5 | 2.9 | 4.4 |
| | UPBE0 | 0.0 | 2.3 | 2.8 | 4.6 |
| | UHF/RHF | 0.4 | 1.7 | 2.2 | 4.1 |
| | UPBE0/RPBE0 | −0.1 | 2.1 | 2.6 | 4.3 |
| | ROHF/RHF | −1.6 | 2.7 | 3.3 | 9.7 |
| SR/MR | UHF | −2.7 | 3.5 | 3.4 | 6.7 |
| | UPBE0 | −2.1 | 2.5 | 2.8 | 7.8 |
| | UHF/RHF | −0.6 | 2.3 | 3.2 | 6.3 |
| | UPBE0/RPBE0 | −2.0 | 2.4 | 2.7 | 7.8 |
| | ROHF/RHF | −3.3 | 3.9 | 4.1 | 10.5 |
| MR | UHF | 8.5 | 12.2 | 13.9 | 31.7 |
| | UPBE0 | −0.7 | 10.3 | 12.9 | 20.3 |
| | UHF/RHF | 7.8 | 8.9 | 6.3 | 12.9 |
| | UPBE0/RPBE0 | −1.1 | 9.9 | 12.3 | 18.2 |
| | ROHF/RHF | −14.6 | 36.6 | 63.8 | 131.9 |
| 3dTMV | UHF | 0.7 | 5.0 | 7.8 | 31.7 |
| | UPBE0 | −0.9 | 4.1 | 6.1 | 20.3 |
| | UHF/RHF | 1.6 | 3.5 | 4.9 | 12.9 |
| | UPBE0/RPBE0 | −1.0 | 3.9 | 5.8 | 18.2 |
| | ROHF/RHF | −5.0 (−2.7) | 10.4 (3.7) | 28.1 (4.3) | 131.9 (14.1) |

For the SR subset, CCSD(T) yields accurate IPs, irrespective of the orbital set employed. All MADs are less than 3 kcal/mol. The CCSD(T)/(UHF/RHF) protocol performs the best, with MAD of 1.7 kcal/mol, and absolute max error of 4.1 kcal/mol. The MADs are only slightly worsened for the SR/MR subset – all except the UHF and the ROHF/RHF orbital choices are still sub 3 kcal/mol – though the maximum errors from UPBE0 orbitals are worsened by 2-3 kcal/mol. The unreasonably large errors, especially as reflected in the MR subset, which result from CCSD(T) with ROHF/RHF references can be traced to a few cases with relatively high multiplicity states (**24**,**25**), which are improperly described at the

ROHF level. In fact, this is a salient reason why we consider the UHF/RHF protocol, which uses RHF for singlets and UHF otherwise.

As expected, CCSD(T) is clearly unreliable for the MR subset, with MADs ranging from 8.9 kcal/mol with the UHF/RHF protocol to 36.6 with RO/R HF orbitals. The maximum absolute errors range from 12.9 to 131.9 kcal/mol. Not only are the majority of IPs far from the ph-AFQMC references, but the sensitivity of the CCSD(T) predictions to the orbital set employed is also dramatically increased (Figure 6 bottom panel). Thus, one clear takeaway from this study is actually in line with the common wisdom that computationally feasible SR methods such as CCSD(T) should not be used for MR systems. Our study confirms this statement, and qualifies it – as we have defined a concrete classification protocol that relies on relatively inexpensive diagnostics.

In all subsets, indeed for the whole 3dTMV set as well, the use of UPBE0 orbitals in CCSD(T) leads to slightly more accurate results than UHF orbitals. This is unsurprising given the large and pervasive artificial SSB at the UHF level (see the SI Table S2). Using restricted orbitals for the singlet states is the simplest way to prevent any spin symmetry breaking (for better or worse), and we find that the CCSD(T)/(UHF/RHF) protocol leads always to more accurate IPs. This is slightly surprising in the context of the MR subset, since one might have expected spin-symmetry breaking, especially at the UPBE0 level, to lead to physically more appropriate electron densities (occupied orbitals). Nevertheless, the present data suggest that the UHF/RHF orbital choice leads to higher accuracy for all 3dTMV subsets.

It is interesting to notice that all metal complexes with bipyridine ligands are classified in the SR/MR set (**15**, **16**, **17**, and **18**). Many aromatic rings such as benzene and naphthalene are substantially spin-contaminated at the UHF level,[149] as are these bipyridine ligand complexes. The SSB from UPBE0 is much reduced vs UHF, and that from CCSD/UPBE0 is much reduced vs CCSD/UHF (this can generally be seen in the SR/MR subset). For the above systems, the calculated IPs from CCSD(T)/UPBE0 are much closer to the ph-

AFQMC values than those from CCSD(T)/UHF. However, there is a small number of cases in the SR/MR set for which CC/UPBE0 reduces the SSB vs CC/UHF but leads to a worse IP. **19** is one such case, and an analysis of the atomic spin densities proves illuminating. For this doublet oxidized state, UHF, although strongly spin-contaminated (see Figure 5**a**), shows in principle the correct electron configuration, i.e., the unpaired electron is metal-centered. Upon introducing dynamic correlation when going to CCSD/UHF (Figure 5**b**), the SSB is significantly reduced and the metal-centered radical can still be observed. In contrast, UPBE0, although almost without any SSB, implies that the radical is centered on the indenyl ligand (Figure 5**c**). Apparently, CC based on this qualitatively incorrect reference cannot recover the expected electron configuration (cf. Figure 4).

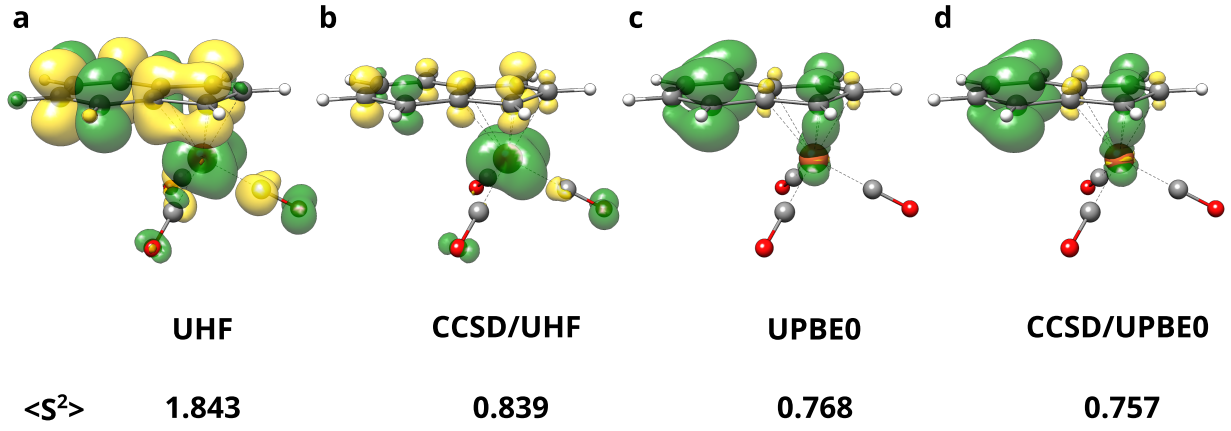


Figure 5: Spin density plots with (**a**) UHF, (**b**) CCSD/UHF, (**c**) UPBE0, and (**d**) CCSD/UPBE0 for the the doublet oxidized state of **19**. $\alpha$ density depicted in green and $\beta$ density in yellow with an isovalue of 0.005 a.u. Mulliken CCSD charge and spin populations are shown in the SI in Table S9.

The effect of the Yamaguchi spin projection[150–153] on UCCSD(T) total energies was systematically investigated for CCSD(T) calculations with UHF, UPBE0, UHF/RHF, and UPBE0/RPBE0 orbitals. The formula for a spin-projected energy of a low-spin state is:

$$E_{LS} = \frac{E_{BS} - (1-\alpha)E_{HS}}{\alpha}, \tag{3}$$

where LS indicates the spin-pure low-spin state, BS indicates the broken symmetry low-spin

state, and HS the high-spin state. The spin-coupling coefficient $\alpha$ is calculated according to

$$\alpha = \frac{\langle S^2 \rangle_{HS} - \langle S^2 \rangle_{BS}}{\langle S^2 \rangle_{HS} - \langle S^2 \rangle_{LS}}. \tag{4}$$

We note that this expression is exact when the BS state can be written as a linear combination of exactly two states – the LS and HS eigenstates. This condition is not generally true, however it is very likely to be applicable when the HS state is spin-pure.

For cases where the CCSD regularized $\langle S^2 \rangle$ deviation is greater than or equal to 2%, the next higher-spin state (HS) (i.e., the original spin multiplicity plus two) was calculated and used in the projection if the HS regularized $\langle S^2 \rangle$ deviation was smaller than or equal to 2% (results utilizing 1, 3, and 4% are similar, and are shown in Section 5.5 of the SI). For IPs in which either the oxidized or the initial state did not agree with these criteria the Yamaguchi spin-projection was not applied for both of these states. The statistical results for spin-projected CCSD(T) with various choices of orbitals, vs the LO-ph-AFQMC reference values, are shown in Table 3. We find that the Yamaguchi projection protocol does not lead to substantial changes in the accuracy statistics. For example, the MAD of CCSD(T) with UHF/RHF orbitals remains at 1.7 kcal/mol for the SR set (although the AMAX is reduced from 4.1 to 3.6) and is reduced from 2.3 to 2.2 kcal/mol in the SR/MR subset. Given the statistical error bars in the LO-ph-AFQMC reference calculations, these changes are not significant. For the MR set, the MAD of 8.9 with UHF/RHF orbitals is slightly reduced to 8.3 kcal/mol, with rather large maximum errors still.

Table 3: Statistical comparison of Yamaguchi corrected CCSD(T) methods.

| Set | CCSD(T) | MD | MAD | SD | AMAX |
|---|---|---|---|---|---|
| SR | UHF+Y | −0.5 | 2.4 | 2.8 | 4.4 |
| | UPBE0+Y | −0.1 | 2.2 | 2.7 | 4.3 |
| | UHF+Y/RHF | 0.3 | 1.7 | 2.2 | 3.6 |
| | UPBE0+Y/RPBE0 | −0.1 | 2.1 | 2.6 | 4.3 |
| SR/MR | UHF+Y | −3.0 | 3.4 | 2.9 | 6.5 |
| | UPBE0+Y | −1.5 | 2.3 | 3.0 | 7.8 |
| | UHF+Y/RHF | −1.4 | 2.2 | 2.8 | 6.3 |
| | UPBE0+Y/RPBE0 | −2.1 | 2.4 | 2.7 | 7.8 |
| MR | UHF+Y | 8.0 | 11.1 | 13.7 | 31.7 |
| | UPBE0+Y | −1.6 | 10.3 | 12.6 | 19.4 |
| | UHF+Y/RHF | 6.6 | 8.3 | 7.4 | 12.9 |
| | UPBE0+Y/RPBE0 | −1.8 | 10.1 | 12.2 | 18.2 |
| 3dTMV | UHF+Y | 0.4 | 4.6 | 7.6 | 31.7 |
| | UPBE0+Y | −0.9 | 4.0 | 6.0 | 19.4 |
| | UHF+Y/RHF | 1.1 | 3.3 | 4.9 | 12.9 |
| | UPBE0+Y/RPBE0 | −1.2 | 3.9 | 5.8 | 18.2 |

The observation that the oxidized states appear to be more MR than the initial states, on average, motivated us to investigate the accuracy of EOM-IP-CCSD. Despite a few technical difficulties (**2**, **4**, **20** which are discussed in the SI in section 5.3), we performed EOM-IP-CCSD calculations with UHF/RHF reference orbitals. Deviations of the predicted vertical IPs vs AFQMC, along with those from CCSD and CCSD(T) with the same UHF/RHF orbital choice, are shown in Figure 6**a** and a statistical summary in Table 4. While EOM-IP-CCSD is slightly more accurate than CCSD (both with UHF/RHF orbitals) for both the SR and SR/MR subsets, we find the opposite for the MR subset. Figure 6b shows the (T) contribution to the IP for each complex, and indeed the cases in the SR and SR/MR subsets in which this is large exhibit notable improvements going from CCSD to CCSD(T) (e.g., complexes **2**, **8**, **14**, **15-18**, **21**). In almost every case, the perturbative triples correction is larger with UKS orbitals than with UHF orbitals (cf. also Figure S2 and Table S11 of the SI). The KS orbitals are recanonicalized prior to subsequent CC calculations, so this finding cannot simply be ascribed to smaller KS eigenvalue differences. While one might

expect that the contribution of triples should correlate with MR character, it appears that it need not, in the sense that there are cases in the SR and SR/MR subsets which have large (T) contributions. Complex **2** shows a (T) contribution in excess of 10 kcal/mol, which appears to be due to the bonded triflate anion. The bipyridines, **15-18**, also have large (T) contributions, as does complex **21** with the bound $N_2$. The latter is consistent with the finding that CCSD makes large errors in the bond dissociation of a system involving a triple-bonded ligand (c.f. $Cu(CO)_4^+$ from Ref. 13). Finally, we find that (T) corrections often play a large role in MR systems. This can be understood by considering the case of a diradicaloid (such as ozone). Double excitations are needed to produce a qualitatively correct open-shell singlet reference, while triples and higher-order excitations are needed to describe the dynamical correlation required for a quantitative description. In these MR transition metal cases, (T) is clearly not enough to describe the relatively large dynamical correlation.

To improve the description of correlation effects beyond CCSD, more sophisticated approximations for connected triples excitations such as the fully renormalized triple correction to CCSD (CR-CC(2,3)) developed by Piecuch *et al.*[133,134] may be needed. The advantage of this method over other approaches that resort to MR concepts to improve the conventional CCSD(T) approach is that it is only at most twice as expensive as the latter. In this work, due to technical restrictions (partly ROHF convergence problems), we computed only four systems (**1**, **2**, **7**, and **9**) from the SR set using the ROHF/RHF based CR-CC(2,3) implementation in GAMESS. As expected, the results for these SR systems are very similar to the ROHF/RHF CCSD(T) results (see Table S16 in the SI). It would be of interest to examine the SR/MR and MR subsets with methods such as CR-CC(2,3) (which would require a robust unrestricted implementation).

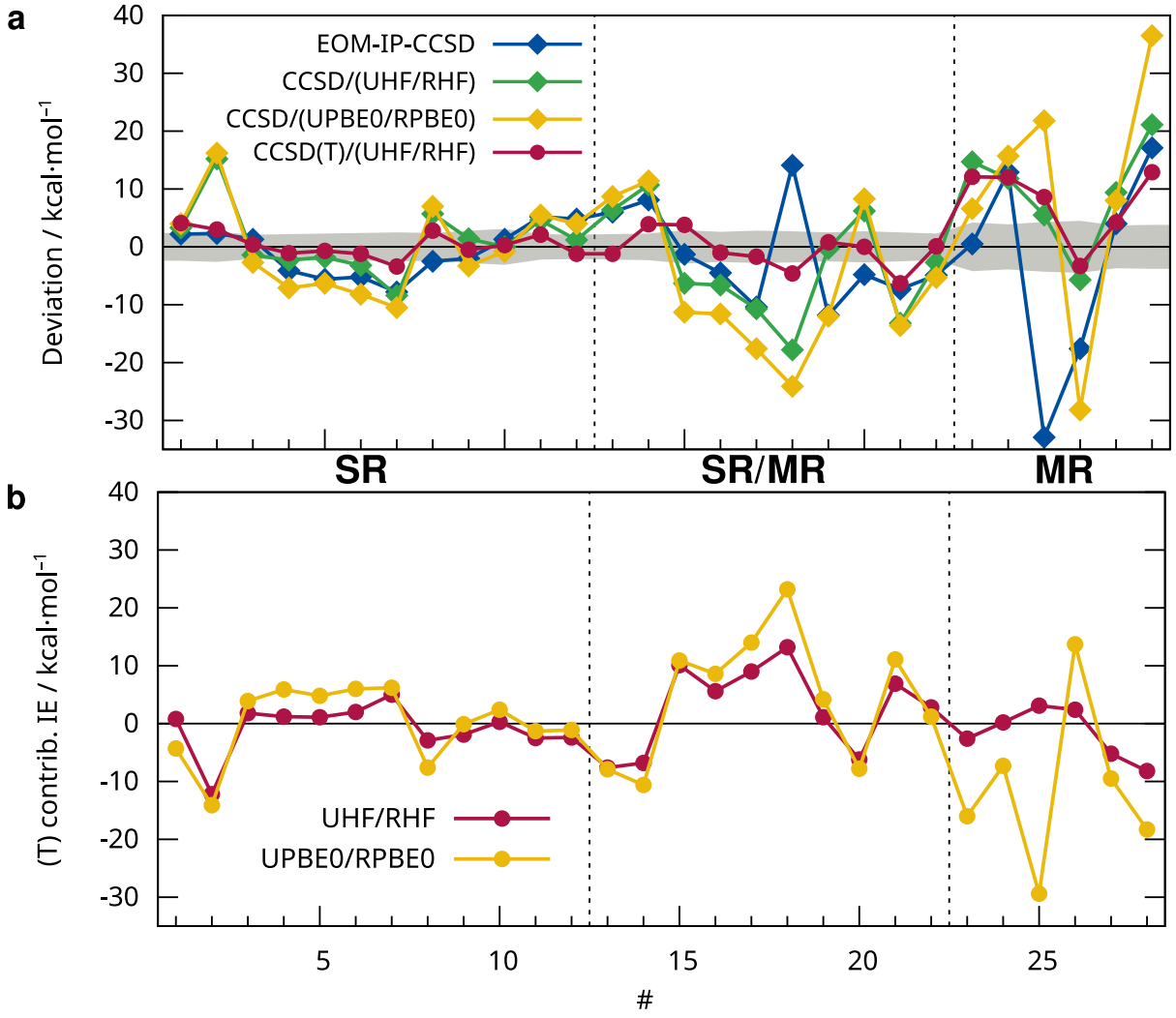


Figure 6: (**a**) Comparison between EOM-IP-CCSD, CCSD, and CCSD(T) on UHF/RHF orbitals with respect to LO-ph-AFQMC. (**b**) Triples contribution (T) for the IPs in CCSD(T) with UHF/RHF and UPBE0/RPBE0 orbitals.

Table 4: Statistical comparison between EOM-IP-CCSD, CCSD and CCSD(T) on UHF/RHF orbitals and CCSD on UPBE0/RPBE0 orbitals with respect to LO-ph-AFQMC.

| Set | Method | MD | MAD | SD | AMAX |
|---|---|---|---|---|---|
| SR | EOM-IP-CCSD/(UHF/RHF) | -0.8 | 3.7 | 4.3 | 7.8 |
| | CCSD/(UHF/RHF) | 1.2 | 4.0 | 5.8 | 15.2 |
| | CCSD/(UPBE0/RPBE0) | −0.2 | 6.3 | 7.7 | 16.2 |
| | CCSD(T)/(UHF/RHF) | 0.4 | 1.7 | 2.2 | 4.1 |
| SR/MR | EOM-IP-CCSD/(UHF/RHF) | −1.7 | 7.3 | 8.4 | 14.1 |
| | CCSD/(UHF/RHF) | −3.4 | 8.1 | 9.3 | 17.8 |
| | CCSD/(UPBE0/RPBE0) | −6.7 | 12.4 | 12.2 | 24.1 |
| | CCSD(T)/(UHF/RHF) | −0.6 | 2.3 | 3.2 | 6.3 |
| MR | EOM-IP-CCSD/(UHF/RHF) | −2.7 | 14.2 | 19.1 | 32.9 |
| | CCSD/(UHF/RHF) | 9.5 | 11.4 | 9.1 | 21.1 |
| | CCSD/(UPBE0/RPBE0) | 10.1 | 19.5 | 21.7 | 36.5 |
| | CCSD(T)/(UHF/RHF) | 7.8 | 8.9 | 6.3 | 12.9 |
| 3dTMV | EOM-IP-CCSD/(UHF/RHF) | −1.5 | 7.2 | 10.0 | 32.9 |
| | CCSD/(UHF/RHF) | 1.3 | 7.1 | 9.0 | 21.1 |
| | CCSD/(UPBE0/RPBE0) | −0.3 | 11.3 | 14.1 | 36.5 |
| | CCSD(T)/(UHF/RHF) | 1.6 | 3.5 | 4.9 | 12.9 |

## 3.4 Preliminary DFT Evaluation

A statistical comparison between various DFT functionals with respect to LO-ph-AFQMC, all evaluated in the def2-SVP basis, is given in Figure 7. Although this comparison is not completely justified because of different degrees of basis set incompleteness error (BSIE) between DFT and orbital-space methods (CC and AFQMC), we present these results as a preliminary indication of how the various DFT functionals are likely to perform.

The MDs of different functionals range from −0.9 kcal/mol for PBE-D4 to 5.9 kcal/mol for ωB97X-V (see SI Table S3-S5 for details). Thus, this preliminary comparison seems to be reasonably appropriate, although a slight trend to positive MDs is observed. The hybrid functional M06-2X yields the largest MAD, which is not surprising because it has been mainly designed for main group chemistry applications. It is followed by the GGA functional PBE-D4 (MAD = 11.3 kcal/mol) and the KP16 hybrid functional (MAD = 10.8 kcal/mol). The

meta-GGAs r$^2$SCAN-D4 and M06-L show an improvement over PBE-D4 with MADs of 8.7 kcal/mol and 7.9 kcal/mol respectively. The hybrid functionals PBE0-D4, r$^2$SCAN0-D4, B3LYP-D4, and PW6B95-D4 all perform relatively well with overall MADs between 7.8 kcal/mol and 6.8 kcal/mol with B3LYP being the best performer. It is noticeable that from these hybrid functionals B3LYP has the smallest amount of Fock exchange (20%). A worse MAD of 9.1 kcal/mol is obtained with $\omega$B97X-V, but an improvement to an MAD of 6.1 kcal/mol is observed when an optimal tuning (OT) procedure is applied for each IP separately (see SI section 4.3 for details), yielding the overall best performing DFT method OT-$\omega$B97X-V. Typical OT-$\omega$ values on this set are around 0.15 and therefore $\omega = 0.15$ as global parameter was also tested yielding the $\omega$B97X15-V method, which yields almost the same overall MAD of 6.2 kcal/mol. The local hybrid functional LH20t-D4 yields an MAD of 7.3 kcal/mol and the double-hybrid PWPB95 an MAD of 7.4 kcal/mol.

On average, as with CCSD(T) methods, the MAD for the SR subset is the smallest followed by those of the SR/MR and MR subsets. While the differences in MAD between the SR and SR/MR subset are small for most functionals, the MAD for the MR subset is between 2-3 times larger than that of the SR/MR subset in most cases. There are two exceptions to this: For the KP16 functional the MR set has an MAD of 14.0 kcal/mol compared to 9.3 kcal/mol for the SR/MR subset the difference is small but the overall performance is already bad compared to the other hybrid functionals. This could be due to the non-self-consistent evaluation on B3LYP orbitals. The other exception is the PWPB95-D4 functional where the SR/MR set has an relatively large MAD of 8.5 kcal/mol and the MR subset has an MAD of 10.9 kcal/mol. In the SR/MR set relatively large errors for the bpy-complexes **15-18** on the order of 10-15 kcal/mol are observed. This is in accordance with the large (T) contribution for these complexes. Apparently higher-order correlation effect that are not covered by the pairwise-additive MP2 part[13,19] in PWPB95-D4 are crucial for these complexes and therefore it fails to produce reliable results.

The Yamaguchi spin projection was also evaluated for DFT with the $\omega$B97X15-V func-

tional. Here, the same criteria as for UCCSD(T) were applied and resulted in a small reduction for the overall MAD from 6.2 kcal/mol to 6.0 kcal/mol.

In order to estimate the remaining BSIE, the PBE0 and the PWPB95 functional were evaluated with the def2-QZVPP basis set and the def2-SVP IPs were compared to these results (See Table S6 in the SI for details). For PBE0 this yields an MD of -0.9 kcal/mol and an MAD of 1.7 kcal/mol relative to the QZ basis with the largest deviation of -3.7 kcal/mol for complex **23**. The double hybrid PWPB95 is expected to be particularly sensitive to the basis set, as a part of its correlation energy is computed by DFT, while the other part is from MP2. Indeed, with PWPB95 this difference is larger and an MD of -3.7 kcal/mol and an MAD of 4.0 kcal/mol is obtained. The largest deviation of -9.3 kcal/mol is obtained for complex **5**. Novel DFT developments such as local hybrids incorporating a strong correlation factor[154] and double-hybrid functionals with regularized MP2[19,155] contribution are interesting candidates for testing on this newly compiled set.

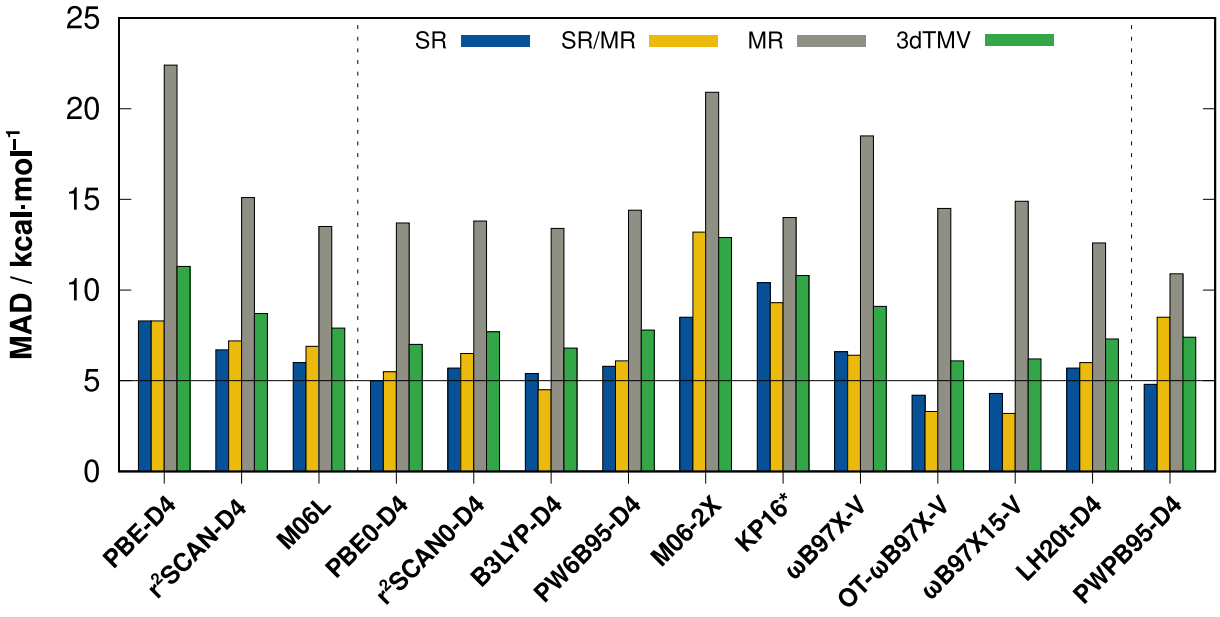


Figure 7: MAD with respect to the LO-ph-AFQMC reference values for the three subsets and the whole 3dTMV set. The KP16 functional could not be evaluated self consistently and was therefore evaluated on B3LYP orbitals.

# 4 Conclusion

Electron transfers involving transition metal catalysts are ubiquitous in chemistry, but are difficult to accurately model with approximate quantum chemical methods due to the presence of both dynamic and static electron correlation. In this regime, the appropriateness of SR CCSD(T) – the "gold standard" computational level for the majority of chemically relevant systems – is still debatable. In the absence of gas-phase experimental values, we leverage the unique scalability and high accuracy of auxiliary-field quantum Monte Carlo to provide reference vertical ionization energies. We compile a set of 28 3d complexes relevant to homogeneous electrocatalysis (which we refer to as 3dTMV), classify them into subsets based on the degree of multi-reference character in the involved states, and assess various CC protocols. Mean absolute deviations roughly equal or less than 2 kcal/mol can be achieved for the predominately SR subsets – namely, with unrestricted/restricted reference orbitals for non-singlet/singlet spin states – and we confirm that CCSD(T) is an inappropriate model for strongly correlated transition metal complexes.

This work demonstrates that one valuable application of AFQMC, which in recent years has undergone rapid development and optimization, is to produce reference values for transition metal thermochemistry. Compared to the CCSD(T) calculations performed in this work, which required wall-times ranging from 2 to 48 hours with 8 cores, LO-ph-AFQMC calculations are relatively more expensive yet can be trivially parallelized. For example, complexes in the SR and SR/MR subsets required between 40 to 150 GPU-node hours, while some MR molecules using trials with the largest active space size took up to 1200 node hours, which corresponds to a wall-time of 12 hours on 96 OLCF Summit nodes). While challenging to converge away the phaseless bias for multi-reference states, in this work we demonstrate that this is possible for realistic mono-metal electrocatalysts at least in a double-zeta basis set. Current work is underway to approach the complete basis set limit, which will be necessary to properly assess and develop approximate density functionals and to compare with gas-phase experiments. We acknowledge that a truly robust and predictive computational protocol

for realistic electrocatalysis must incorporate solvation free-energies and finite-temperature effects – from this perspective, the present work is a promising first step.

Another notable achievement is that we have pinpointed quantitative metrics based on symmetry breaking and the largest coefficient in selected CI multi-determinant expansions, which are meaningful and effective in diagnosing MR character. Specifically, we propose thresholds for spin-symmetry breaking from unrestricted CCSD and KS-PBE0 along with the metric $1-C_0^2$ from ph-AFQMC trial wavefunctions, which can delineate regimes inside of which appropriately-performed CCSD(T) can produce $< 2.3$ kcal/mol accuracy, and outside of which CCSD(T) with the investigated choices of orbitals can be expected to fail. Our analysis of the many MR diagnostics proposed in the literature suggest that $\langle S^2 \rangle_{PBE0}$ is a computationally-inexpensive proxy which, while admittedly not rigorous, is herein found empirically to be practically useful in assessing the regime of applicability of CCSD(T) methods.

Among the many implications of this work on best-practices in quantum chemistry for transition metal systems, we propose that for target molecules which can be classified as SR or SR/MR, the agreement of ph-AFQMC and CCSD(T) with UHF/RHF orbitals can be expected, and consensus predictions ought to be more reliable than predictions from one of the two methods alone. In fact, occasionally in this work CCSD(T) IPs were used to guide the choice of CASSCF or HCISCF trial wavefunction used in ph-AFQMC; indeed, while a MCSCF optimization may converge to a qualitatively incorrect local minimum that is "closest" to the reference state used to initialize the calculation – thus inheriting an electronic state with, e.g., unphysical spatial symmetry – the $\hat{T}_1$ operator in the CC ansatz makes CCSD(T) relatively less sensitive to the reference used.

The exciting development of localized orbital approximations such as, e.g., the PNO-LCCSD(T)-F12[156] and the DLPNO-CCSD(T) implementations,[42–44] when appropriately converged,[51] can also be readily used in these regimes to provide reliable reference values. With these localized coupled cluster implementations, the use of extended basis sets

is possible and thus a more realistic evaluation of DFT methods as well as a comparison with experimentally measured ionization energies. Our (preliminary) evaluation of selected DFT functionals in a rather smaller basis set revealed that $\omega$B97X-V with a lowered $\omega$ value of 0.15 may be well suited for application in computational studies involving 3d transition metal electrocatalysts.

Finally, we remark that large, orbital-dependent triples contributions for complexes with, e.g., triflate and fluorine atoms, bipyridine, $N_2$ (triple bond) provide new opportunities to assess alternate and develop improved approximate triples variants in the SR and SR/MR correlation regime, such as the renormalized coupled cluster methods.[133,134]

In summary, we have taken important first steps towards the reliable modeling of chemically-relevant 3d TM electrocatalysts. We envision that future improvements in CC and AFQMC methods, used in combination with effective MR diagnostics and solvation models, can be used to predict reference-quality thermochemical values involving electronic states spanning a wide variety of correlation regimes. The curation of new transition metal datasets will also accelerate the development of faster quantum chemical or data-driven methods as well.

## Acknowledgement

The German Science Foundation (DFG) is gratefully acknowledged for financial support (Grant 1927/16-1). This research used resources of the Oak Ridge Leadership Computing Facility at the Oak Ridge National Laboratory, which is supported by the Office of Science of the U.S. Department of Energy under Contract DE-AC05-00OR22725. This work used the Extreme Science and Engineering Discovery Environment (XSEDE), which is supported by National Science Foundation grant number ACI-1548562. Calculations used the XSEDE resource Expanse at the SDSC through allocation ID COL151. J.S. acknowledges funding from the National Institute of General Medical Sciences of the National Institutes of Health under award number F32GM142231. This research used resources of the National Energy

Research Scientific Computing Center (NERSC), a U.S. Department of Energy Office of Science User Facility located at Lawrence Berkeley National Laboratory. We are thankful to Achintya Kumar Dutta for stimulating discussion and helpful advice about EOM-CCSD methods and to Stefan Grimme for proofreading. We greatly acknowledge the help from Piotr Piecuch, Jun Shen, and Jorge Deustua concerning the CR-CC(2,3) calculations. Furthermore, the authors thank Demyan Prokopchuk for helpful literature recommendations, Jing Kong for providing the xTron code and for technical support with setting it up, and James Smith for useful discussions about HCISCF. We acknowledged the Bill and Melinda Gates Foundations.

## Supporting Information Available

The following files are available free of charge.

- 3dtmv.zip: Cartesian coordinates of the 3dTMV
- si.pdf: IPs of all CC and ph-AFQMC calculations, contribution of (T) to CCSD(T) correlation energy, IPs and statistics for Yamaguchi projection with CCSD(T), basis set study and statistics with DFT, additional details of LO-ph-AFQMC calculations
- data.xlsx: DFT IPs, raw data for the PCA, OT-omega values

## References

(1) Francke, R.; Little, R. D. Redox catalysis in organic electrosynthesis: basic principles and recent developments. *Chem. Soc. Rev.* **2014**, *43*, 2492–2521.

(2) Siu, J. C.; Fu, N.; Lin, S. Catalyzing Electrosynthesis: A Homogeneous Electrocatalytic Approach to Reaction Discovery. *Acc. Chem. Res.* **2020**, *53*, 547–560, PMID: 32077681.

(3) Benson, E. E.; Kubiak, C. P.; Sathrum, A. J.; Smieja, J. M. Electrocatalytic and homogeneous approaches to conversion of CO2 to liquid fuels. *Chem. Soc. Rev.* **2009**, *38*, 89–99.

(4) Francke, R.; Schille, B.; Roemelt, M. Homogeneously Catalyzed Electroreduction of Carbon Dioxide—Methods, Mechanisms, and Catalysts. *Chem. Rev.* **2018**, *118*, 4631–4701, PMID: 29319300.

(5) Dalle, K. E.; Warnan, J.; Leung, J. J.; Reuillard, B.; Karmel, I. S.; Reisner, E. Electro- and Solar-Driven Fuel Synthesis with First Row Transition Metal Complexes. *Chem. Rev.* **2019**, *119*, 2752–2875, PMID: 30767519.

(6) Kinzel, N. W.; Werlé, C.; Leitner, W. Transition Metal Complexes as Catalysts for the Electroconversion of CO2: An Organometallic Perspective. *Angew. Chem. Int. Ed.* **2021**, *60*, 11628–11686.

(7) Artero, V.; Chavarot-Kerlidou, M.; Fontecave, M. Splitting Water with Cobalt. *Angew. Chem. Int. Ed.* **2011**, *50*, 7238–7266.

(8) Du, P.; Eisenberg, R. Catalysts made of earth-abundant elements (Co, Ni, Fe) for water splitting: Recent progress and future challenges. *Energy Environ. Sci.* **2012**, *5*, 6012–6021.

(9) Pegis, M. L.; Wise, C. F.; Martin, D. J.; Mayer, J. M. Oxygen Reduction by Homogeneous Molecular Catalysts and Electrocatalysts. *Chem. Rev.* **2018**, *118*, 2340–2391, PMID: 29406708.

(10) Luo, G.-G.; Zhang, H.-L.; Tao, Y.-W.; Wu, Q.-Y.; Tian, D.; Zhang, Q. Recent progress in ligand-centered homogeneous electrocatalysts for hydrogen evolution reaction. *Inorg. Chem. Front.* **2019**, *6*, 343–354.

(11) Bullock, R. M.; Chen, J. G.; Gagliardi, L.; Chirik, P. J.; Farha, O. K.; Hendon, C. H.; Jones, C. W.; Keith, J. A.; Klosin, J.; Minteer, S. D.; Morris, R. H.; Radosevich, A. T.; Rauchfuss, T. B.; Strotman, N. A.; Vojvodic, A.; Ward, T. R.; Yang, J. Y.; Surendranath, Y. Using nature's blueprint to expand catalysis with Earth-abundant metals. *Science* **2020**, *369*, eabc3183.

(12) Vogiatzis, K. D.; Polynski, M. V.; Kirkland, J. K.; Townsend, J.; Hashemi, A.; Liu, C.; Pidko, E. A. Computational Approach to Molecular Catalysis by 3d Transition Metals: Challenges and Opportunities. *Chem. Rev.* **2019**, *119*, 2453–2523, PMID: 30376310.

(13) Shee, J.; Loipersberger, M.; Hait, D.; Lee, J.; Head-Gordon, M. Revealing the nature of electron correlation in transition metal complexes with symmetry breaking and chemical intuition. *J. Chem. Phys.* **2021**, *154*, 194109.

(14) Jiang, W.; DeYonker, N. J.; Wilson, A. K. Multireference Character for 3d Transition-Metal-Containing Molecules. *J. Chem. Theory Comput.* **2012**, *8*, 460–468, PMID: 26596596.

(15) Khedkar, A.; Roemelt, M. Modern multireference methods and their application in transition metal chemistry. *Phys. Chem. Chem. Phys.* **2021**, *23*, 17097–17112.

(16) Rastetter, U.; Jacobi von Wangelin, A.; Herrmann, C. Redox-active ligands as a challenge for electronic structure methods. *J. Comput. Chem.* **2023**, *44*, 468–479.

(17) Süß, D.; Huber, S. E.; Mauracher, A. On the impact of multi-reference character of small transition metal compounds on their bond dissociation energies. *J. Chem. Phys.* **2020**, *152*, 114104.

(18) Duan, C.; Chu, D. B. K.; Nandy, A.; Kulik, H. J. Detection of multi-reference character imbalances enables a transfer learning approach for virtual high throughput screening with coupled cluster accuracy at DFT cost. *Chem. Sci.* **2022**, *13*, 4962–4971.

(19) Shee, J.; Loipersberger, M.; Rettig, A.; Lee, J.; Head-Gordon, M. Regularized Second-Order Møller–Plesset Theory: A More Accurate Alternative to Conventional MP2 for Noncovalent Interactions and Transition Metal Thermochemistry for the Same Computational Cost. *J. Phys. Chem. Lett.* **2021**, *12*, 12084–12097, PMID: 34910484.

(20) Rettig, A.; Shee, J.; Lee, J.; Head-Gordon, M. Revisiting the Orbital Energy-Dependent Regularization of Orbital-Optimized Second-Order Møller–Plesset Theory. *J. Chem. Theory Comput.* **2022**, *18*, 5382–5392, PMID: 36050889.

(21) Marenich, A. V.; Ho, J.; Coote, M. L.; Cramer, C. J.; Truhlar, D. G. Computational electrochemistry: prediction of liquid-phase reduction potentials. *Phys. Chem. Chem. Phys.* **2014**, *16*, 15068–15106.

(22) Galstyan, A.; Knapp, E.-W. Accurate redox potentials of mononuclear iron, manganese, and nickel model complexes. *J. Comput. Chem.* **2009**, *30*, 203–211.

(23) Roy, L. E.; Jakubikova, E.; Guthrie, M. G.; Batista, E. R. Calculation of One-Electron Redox Potentials Revisited. Is It Possible to Calculate Accurate Potentials with Density Functional Methods? *J. Phys. Chem. A* **2009**, *113*, 6745–6750, PMID: 19459608.

(24) Konezny, S. J.; Doherty, M. D.; Luca, O. R.; Crabtree, R. H.; Soloveichik, G. L.; Batista, V. S. Reduction of Systematic Uncertainty in DFT Redox Potentials of Transition-Metal Complexes. *J. Phys. Chem. C* **2012**, *116*, 6349–6356.

(25) Coskun, D.; Jerome, S. V.; Friesner, R. A. Evaluation of the Performance of the B3LYP, PBE0, and M06 DFT Functionals, and DBLOC-Corrected Versions, in the Calculation of Redox Potentials and Spin Splittings for Transition Metal Containing Systems. *J. Chem. Theory Comput.* **2016**, *12*, 1121–1128, PMID: 26808695.

(26) Neugebauer, H.; Bohle, F.; Bursch, M.; Hansen, A.; Grimme, S. Benchmark Study of Electrochemical Redox Potentials Calculated with Semiempirical and DFT Methods. *J. Phys. Chem. A* **2020**, *124*, 7166–7176, PMID: 32786975.

(27) Isegawa, M.; Neese, F.; Pantazis, D. A. Ionization Energies and Aqueous Redox Potentials of Organic Molecules: Comparison of DFT, Correlated ab Initio Theory and Pair Natural Orbital Approaches. *J. Chem. Theory Comput.* **2016**, *12*, 2272–2284, PMID: 27065224.

(28) Sterling, C. M.; Bjornsson, R. Multistep Explicit Solvation Protocol for Calculation of Redox Potentials. *J. Chem. Theory Comput.* **2019**, *15*, 52–67.

(29) Bhattacharjee, S.; Isegawa, M.; Garcia-Ratés, M.; Neese, F.; Pantazis, D. A. Ionization Energies and Redox Potentials of Hydrated Transition Metal Ions: Evaluation of Domain-Based Local Pair Natural Orbital Coupled Cluster Approaches. *J. Chem. Theory Comput.* **2022**, *18*, 1619–1632, PMID: 35191695.

(30) Bartlett, R. J.; Musiał, M. Coupled-cluster theory in quantum chemistry. *Rev. Mod. Phys.* **2007**, *79*, 291–352.

(31) Richard, R. M.; Marshall, M. S.; Dolgounitcheva, O.; Ortiz, J. V.; Brédas, J.-L.; Marom, N.; Sherrill, C. D. Accurate Ionization Potentials and Electron Affinities of Acceptor Molecules I. Reference Data at the CCSD(T) Complete Basis Set Limit. *J. Chem. Theory Comput.* **2016**, *12*, 595–604, PMID: 26731487.

(32) Shee, J.; Arthur, E. J.; Zhang, S.; Reichman, D. R.; Friesner, R. A. Phaseless Auxiliary-Field Quantum Monte Carlo on Graphical Processing Units. *J. Chem. Theory Comput.* **2018**, *14*, 4109–4121, PMID: 29897748.

(33) Jiang, W.; DeYonker, N. J.; Determan, J. J.; Wilson, A. K. Toward Accurate Theoretical Thermochemistry of First Row Transition Metal Complexes. *J. Phys. Chem. A* **2012**, *116*, 870–885, PMID: 22107449.

(34) Fang, Z.; Vasiliu, M.; Peterson, K. A.; Dixon, D. A. Prediction of Bond Dissociation Energies/Heats of Formation for Diatomic Transition Metal Compounds: CCSD(T) Works. *J. Chem. Theory Comput.* **2017**, *13*, 1057–1066, PMID: 28080051.

(35) Cheng, L.; Gauss, J.; Ruscic, B.; Armentrout, P. B.; Stanton, J. F. Bond Dissociation Energies for Diatomic Molecules Containing 3d Transition Metals: Benchmark Scalar-Relativistic Coupled-Cluster Calculations for 20 Molecules. *J. Chem. Theory Comput.* **2017**, *13*, 1044–1056, PMID: 28080054.

(36) Aoto, Y. A.; de Lima Batista, A. P.; Köhn, A.; de Oliveira-Filho, A. G. S. How To Arrive at Accurate Benchmark Values for Transition Metal Compounds: Computation or Experiment? *J. Chem. Theory Comput.* **2017**, *13*, 5291–5316, PMID: 28953375.

(37) Shee, J.; Rudshteyn, B.; Arthur, E. J.; Zhang, S.; Reichman, D. R.; Friesner, R. A. On Achieving High Accuracy in Quantum Chemical Calculations of 3d Transition Metal-Containing Systems: A Comparison of Auxiliary-Field Quantum Monte Carlo with Coupled Cluster, Density Functional Theory, and Experiment for Diatomic Molecules. *J. Chem. Theory Comput.* **2019**, *15*, 2346–2358, PMID: 30883110.

(38) Hait, D.; Tubman, N. M.; Levine, D. S.; Whaley, K. B.; Head-Gordon, M. What Levels of Coupled Cluster Theory Are Appropriate for Transition Metal Systems? A Study Using Near-Exact Quantum Chemical Values for 3d Transition Metal Binary Compounds. *J. Chem. Theory Comput.* **2019**, *15*, 5370–5385, PMID: 31465217.

(39) Radoń, M. Benchmarking quantum chemistry methods for spin-state energetics of iron complexes against quantitative experimental data. *Phys. Chem. Chem. Phys.* **2019**, *21*, 4854–4870.

(40) Drabik, G.; Szklarzewicz, J.; Radoń, M. Spin-state energetics of metallocenes: How do best wave function and density functional theory results compare with the experimental data? *Phys. Chem. Chem. Phys.* **2021**, *23*, 151–172.

(41) Bertels, L. W.; Lee, J.; Head-Gordon, M. Polishing the Gold Standard: The Role of Orbital Choice in CCSD(T) Vibrational Frequency Prediction. *J. Chem. Theory Comput.* **2021**, *17*, 742–755, PMID: 33404238.

(42) Hansen, A.; Liakos, D. G.; Neese, F. Efficient and accurate local single reference correlation methods for high-spin open-shell molecules using pair natural orbitals. *J. Chem. Phys.* **2011**, *135*, 214102.

(43) Saitow, M.; Becker, U.; Riplinger, C.; Valeev, E. F.; Neese, F. A new near-linear scaling, efficient and accurate, open-shell domain-based local pair natural orbital coupled cluster singles and doubles theory. *J. Chem. Phys.* **2017**, *146*, 164105.

(44) Riplinger, C.; Sandhoefer, B.; Hansen, A.; Neese, F. Natural triple excitations in local coupled cluster calculations with pair natural orbitals. *J. Chem. Phys.* **2013**, *139*, 134101.

(45) Dohm, S.; Hansen, A.; Steinmetz, M.; Grimme, S.; Checinski, M. P. Comprehensive Thermochemical Benchmark Set of Realistic Closed-Shell Metal Organic Reactions. *J. Chem. Theory Comput.* **2018**, *14*, 2596–2608, PMID: 29565586.

(46) Maurer, L. R.; Bursch, M.; Grimme, S.; Hansen, A. Assessing Density Functional Theory for Chemically Relevant Open-Shell Transition Metal Reactions. *J. Chem. Theory Comput.* **2021**, *17*, 6134–6151, PMID: 34546754.

(47) Wappett D, Goerigk L. Benchmarking Density Functional Theory Methods for Metalloenzyme Reactions: The Introduction of the MME55 Set. ChemRxiv. Cambridge: Cambridge Open Engage; 2023; This content is a preprint and has not been peer-reviewed.

(48) Iron, M. A.; Janes, T. Evaluating Transition Metal Barrier Heights with the Latest Density Functional Theory Exchange–Correlation Functionals: The MOBH35 Benchmark Database. *J. Phys. Chem. A* **2019**, *123*, 3761–3781, PMID: 30973722.

(49) Iron, M. A.; Janes, T. Correction to "Evaluating Transition Metal Barrier Heights with the Latest Density Functional Theory Exchange–Correlation Functionals: The

MOBH35 Benchmark Database". *J. Phys. Chem. A* **2019**, *123*, 6379–6380, PMID: 31306024.

(50) Semidalas, E.; Martin, J. M. The MOBH35 Metal–Organic Barrier Heights Reconsidered: Performance of Local-Orbital Coupled Cluster Approaches in Different Static Correlation Regimes. *J. Chem. Theory Comput.* **2022**, *18*, 883–898, PMID: 35045709.

(51) Altun, A.; Riplinger, C.; Neese, F.; Bistoni, G. Exploring the Accuracy Limits of PNO-Based Local Coupled-Cluster Calculations for Transition-Metal Complexes. *J. Chem. Theory Comput.* **2023**, *19*, 2039–2047, PMID: 36917767.

(52) Drosou, M.; Mitsopoulou, C. A.; Pantazis, D. A. Reconciling Local Coupled Cluster with Multireference Approaches for Transition Metal Spin-State Energetics. *J. Chem. Theory Comput.* **2022**, *18*, 3538–3548, PMID: 35582788.

(53) Aðalsteinsson, H. M.; Bjornsson, R. Ionization energies of metallocenes: A coupled cluster study of cobaltocene. *Phys. Chem. Chem. Phys.* **2023**, –.

(54) Shee, J.; Zhang, S.; Reichman, D. R.; Friesner, R. A. Chemical Transformations Approaching Chemical Accuracy via Correlated Sampling in Auxiliary-Field Quantum Monte Carlo. *J. Chem. Theory Comput.* **2017**, *13*, 2667–2680, PMID: 28481546.

(55) Shi, H.; Zhang, S. Some recent developments in auxiliary-field quantum Monte Carlo for real materials. *J. Chem. Phys.* **2021**, *154*, 024107.

(56) Lee, J.; Pham, H. Q.; Reichman, D. R. Twenty Years of Auxiliary-Field Quantum Monte Carlo in Quantum Chemistry: An Overview and Assessment on Main Group Chemistry and Bond-Breaking. *J. Chem. Theory Comput.* **2022**, *18*, 7024–7042, PMID: 36255074.

(57) Shee, J.; Weber, J. L.; Reichman, D. R.; Friesner, R. A.; Zhang, S. On the potentially transformative role of auxiliary-field quantum Monte Carlo in quantum chemistry: A

highly accurate method for transition metals and beyond. *J. Chem. Phys.* **2023**, *158*, 140901.

(58) Zhang, S.; Krakauer, H. Quantum Monte Carlo Method using Phase-Free Random Walks with Slater Determinants. *Phys. Rev. Lett.* **2003**, *90*, 136401.

(59) Al-Saidi, W. A.; Zhang, S.; Krakauer, H. Auxiliary-field quantum Monte Carlo calculations of molecular systems with a Gaussian basis. *J. Chem. Phys.* **2006**, *124*, 224101.

(60) Weber, J. L.; Vuong, H.; Devlaminck, P. A.; Shee, J.; Lee, J.; Reichman, D. R.; Friesner, R. A. A Localized-Orbital Energy Evaluation for Auxiliary-Field Quantum Monte Carlo. *J. Chem. Theory Comput.* **2022**, *18*, 3447–3459, PMID: 35507769.

(61) Malone, F. D.; Zhang, S.; Morales, M. A. Accelerating Auxiliary-Field Quantum Monte Carlo Simulations of Solids with Graphical Processing Units. *J. Chem. Theory Comput.* **2020**, *16*, 4286–4297.

(62) Rudshteyn, B.; Coskun, D.; Weber, J. L.; Arthur, E. J.; Zhang, S.; Reichman, D. R.; Friesner, R. A.; Shee, J. Predicting Ligand-Dissociation Energies of 3d Coordination Complexes with Auxiliary-Field Quantum Monte Carlo. *J. Chem. Theory Comput.* **2020**, *16*, 3041–3054, PMID: 32293882.

(63) Rudshteyn, B.; Weber, J. L.; Coskun, D.; Devlaminck, P. A.; Zhang, S.; Reichman, D. R.; Shee, J.; Friesner, R. A. Calculation of Metallocene Ionization Potentials via Auxiliary Field Quantum Monte Carlo: Toward Benchmark Quantum Chemistry for Transition Metals. *J. Chem. Theory Comput.* **2022**, *18*, 2845–2862, PMID: 35377642.

(64) Reimann, M.; Kaupp, M. Spin-State Splittings in 3d Transition-Metal Complexes Revisited: Benchmarking Approximate Methods for Adiabatic Spin-State Energy Dif-

ferences in Fe(II) Complexes. *J. Chem. Theory Comput.* **2022**, *18*, 7442–7456, PMID: 36417564.

(65) Reimann, M.; Kaupp, M. Spin-State Splittings in 3d Transition-Metal Complexes Revisited: Toward a Reliable Theory Benchmark. *J. Chem. Theory Comput.* **2023**, *19*, 97–108, PMID: 36576816.

(66) Verplancke, H.; Diefenbach, M.; Lienert, J. N.; Ugandi, M.; Kitsaras, M.-P.; Roemelt, M.; Stopkowicz, S.; Holthausen, M. C. Another Torture Track for Quantum Chemistry: Reinvestigation of the Benzaldehyde Amidation by Nitrogen-Atom Transfer from Platinum(II) and Palladium(II) Metallonitrenes. *Isr. J. Chem. n/a*, e202300060.

(67) Grice, K. A.; Saucedo, C.; Sovereign, M. A.; Cho, A. P. The Electrochemical Behavior of Early Metal Metallocene $Cp_2MCl_2$ Complexes under $CO_2$. *Electrochim. Acta* **2016**, *218*, 110–118.

(68) Kessler, M.; Hansen, S.; Hollmann, D.; Klahn, M.; Beweries, T.; Spannenberg, A.; Brückner, A.; Rosenthal, U. Synthesis of $Cp^*_2$Ti(OTf) and Its Reaction with Water. *Eur. J. Inorg. Chem* **2011**, *2011*, 627–631.

(69) Gagne, R. R.; Koval, C. A.; Lisensky, G. C. Ferrocene as an internal standard for electrochemical measurements. *Inorg. Chem.* **1980**, *19*, 2854–2855.

(70) Bond, A. M.; Oldham, K. B.; Snook, G. A. Use of the Ferrocene Oxidation Process To Provide Both Reference Electrode Potential Calibration and a Simple Measurement (via Semiintegration) of the Uncompensated Resistance in Cyclic Voltammetric Studies in High-Resistance Organic Solvents. *Anal. Chem.* **2000**, *72*, 3492–3496, PMID: 10952533.

(71) Namazian, M.; Lin, C. Y.; Coote, M. L. Benchmark Calculations of Absolute Reduc-

tion Potential of Ferricinium/Ferrocene Couple in Nonaqueous Solutions. *J. Chem. Theory Comput.* **2010**, *6*, 2721–2725, PMID: 26616073.

(72) Astruc, D. Why is Ferrocene so Exceptional? *Eur. J. Inorg. Chem.* **2017**, *2017*, 6–29.

(73) Sethi, S.; Das, P. K.; Behera, N. The chemistry of aminoferrocene, Fe($\eta$5-C5H4NH2)($\eta$5-Cp): Synthesis, reactivity and applications. *J. Organomet. Chem.* **2016**, *824*, 140–165.

(74) Goodwin, C. A. P.; Giansiracusa, M. J.; Greer, S. M.; Nicholas, H. M.; Evans, P.; Vonci, M.; Hill, S.; Chilton, N. F.; Mills, D. P. Isolation and electronic structures of derivatized manganocene, ferrocene and cobaltocene anions. *Nat. Chem.* **2021**, *13*, 243–248.

(75) Walawalkar, M. G.; Pandey, P.; Murugavel, R. The Redox Journey of Iconic Ferrocene: Ferrocenium Dications and Ferrocenate Anions. *Angew. Chem. Int. Ed.* **2021**, *60*, 12632–12635.

(76) Artero, V.; Fontecave, M. Hydrogen evolution catalyzed by CpFe(CO)2-based complexes. *C.R. Chim.* **2008**, *11*, 926–931.

(77) Pevear, K. A.; Holl, M. M. B.; Carpenter, G. B.; Rieger, A. L.; Rieger, P. H.; Sweigart, D. A. Ligand Substitution at 19-Electron Centers and the Indenyl Effect in Organometallic Radicals. Electrocatalytic CO Substitution in (cyclopentadienyl)Fe(CO)3+ and (indenyl)Fe(CO)3+. *Organometallics* **1995**, *14*, 512–523.

(78) Rosas-Hernández, A.; Junge, H.; Beller, M.; Roemelt, M.; Francke, R. Cyclopentadienone iron complexes as efficient and selective catalysts for the electroreduction of $CO_2$ to CO. *Catal. Sci. Technol.* **2017**, *7*, 459–465.

(79) Sánchez, P.; Goel, B.; Neugebauer, H.; Lalancette, R. A.; Grimme, S.; Hansen, A.; Prokopchuk, D. E. Ligand Protonation at Carbon, not Nitrogen, during $H_2$ Production

with Amine-Rich Iron Electrocatalysts. *Inorg. Chem.* **2021**, *60*, 17407–17413, PMID: 34735115.

(80) Fang, M.; Wiedner, E. S.; Dougherty, W. G.; Kassel, W. S.; Liu, T.; DuBois, D. L.; Bullock, R. M. Cobalt Complexes Containing Pendant Amines in the Second Coordination Sphere as Electrocatalysts for H2 Production. *Organometallics* **2014**, *33*, 5820–5833.

(81) Craig, C. A.; Spreer, L. O.; Otvos, J. W.; Calvin, M. Photochemical reduction of carbon dioxide using nickel tetraazamacrocycles. *J. Phys. Chem.* **1990**, *94*, 7957–7960.

(82) Helm, M. L.; Stewart, M. P.; Bullock, R. M.; DuBois, M. R.; DuBois, D. L. A Synthetic Nickel Electrocatalyst with a Turnover Frequency Above 100,000 s-1 for $H_2$ Production. *Science* **2011**, *333*, 863–866.

(83) Tory, J.; Setterfield-Price, B.; Dryfe, R. A. W.; Hartl, F. [$M(CO)_4$(2,2'-bipyridine)] (M=Cr, Mo, W) Complexes as Efficient Catalysts for Electrochemical Reduction of $CO_2$ at a Gold Electrode. *ChemElectroChem* **2015**, *2*, 213–217.

(84) Machan, C. W.; Stanton, C. J.; Vandezande, J. E.; Majetich, G. F.; Schaefer, H. F.; Kubiak, C. P.; Agarwal, J. Electrocatalytic Reduction of Carbon Dioxide by Mn(CN)(2,2'-bipyridine)$(CO)_3$: CN Coordination Alters Mechanism. *Inorg. Chem.* **2015**, *54*, 8849–8856, PMID: 26288172.

(85) Alsabeh, P. G.; Rosas-Hernández, A.; Barsch, E.; Junge, H.; Ludwig, R.; Beller, M. Iron-catalyzed photoreduction of carbon dioxide to synthesis gas. *Catal. Sci. Technol.* **2016**, *6*, 3623–3630.

(86) Garnier, L.; Rollin, Y.; Périchon, J. Electrosynthesis of symmetrical ketones from organic halides and carbon dioxide catalysed by 2,2'-bipyridine-nickel complexes. *J. Organomet. Chem.* **1989**, *367*, 347–358.

(87) Razavet, M.; Artero, V.; Fontecave, M. Proton Electroreduction Catalyzed by Cobaloximes: Functional Models for Hydrogenases. *Inorg. Chem.* **2005**, *44*, 4786–4795, PMID: 15962987.

(88) Du, P.; Schneider, J.; Luo, G.; Brennessel, W. W.; Eisenberg, R. Visible Light-Driven Hydrogen Production from Aqueous Protons Catalyzed by Molecular Cobaloxime Catalysts. *Inorg. Chem.* **2009**, *48*, 4952–4962, PMID: 19397296.

(89) Dempsey, J. L.; Brunschwig, B. S.; Winkler, J. R.; Gray, H. B. Hydrogen Evolution Catalyzed by Cobaloximes. *Acc. Chem. Res.* **2009**, *42*, 1995–2004, PMID: 19928840.

(90) Dolui, D.; Khandelwal, S.; Majumder, P.; Dutta, A. The odyssey of cobaloximes for catalytic $H_2$ production and their recent revival with enzyme-inspired design. *Chem. Commun.* **2020**, *56*, 8166–8181.

(91) Kuriyama, S.; Arashiba, K.; Nakajima, K.; Matsuo, Y.; Tanaka, H.; Ishii, K.; Yoshizawa, K.; Nishibayashi, Y. Catalytic transformation of dinitrogen into ammonia and hydrazine by iron-dinitrogen complexes bearing pincer ligand. *Nat. Commun.* **2016**, *7*, 12181.

(92) Beyler, M.; Ezzaher, S.; Karnahl, M.; Santoni, M.-P.; Lomoth, R.; Ott, S. Pentacoordinate iron complexes as functional models of the distal iron in [FeFe] hydrogenases. *Chem. Commun.* **2011**, *47*, 11662–11664.

(93) Lindroth, R.; Ondrejková, A.; Wallentin, C.-J. Visible-Light Mediated Oxidative Fragmentation of Ethers and Acetals by Means of Fe(III) Catalysis. *Organic Letters* **2022**, *24*, 1662–1667, PMID: 35192351.

(94) Felton, G. A. N.; Vannucci, A. K.; Chen, J.; Lockett, L. T.; Okumura, N.; Petro, B. J.; Zakai, U. I.; Evans, D. H.; Glass, R. S.; Lichtenberger, D. L. Hydrogen Generation from Weak Acids: Electrochemical and Computational Studies of a Diiron Hydrogenase Mimic. *J. Am. Chem. Soc.* **2007**, *129*, 12521–12530, PMID: 17894491.

(95) McNamara, W. R.; Han, Z.; Alperin, P. J.; Brennessel, W. W.; Holland, P. L.; Eisenberg, R. A Cobalt–Dithiolene Complex for the Photocatalytic and Electrocatalytic Reduction of Protons. *J. Am. Chem. Soc.* **2011**, *133*, 15368–15371, PMID: 21863808.

(96) Das, A.; Han, Z.; Brennessel, W. W.; Holland, P. L.; Eisenberg, R. Nickel Complexes for Robust Light-Driven and Electrocatalytic Hydrogen Production from Water. *ACS Catal.* **2015**, *5*, 1397–1406.

(97) Ray, K.; DeBeer George, S.; Solomon, E. I.; Wieghardt, K.; Neese, F. Description of the Ground-State Covalencies of the Bis(dithiolato) Transition-Metal Complexes from X-ray Absorption Spectroscopy and Time-Dependent Density-Functional Calculations. *Chem. Eur. J.* **2007**, *13*, 2783–2797.

(98) Bard, A. J.; Garcia, E.; Kukharenko, S.; Strelets, V. V. Electrochemistry of metallocenes at very negative and very positive potentials. Electrogeneration of 17-electron $Cp_2Co^{2+}$, 21-electron $Cp_2Co^{2-}$, and 22-electron $Cp_2Ni^{2-}$ species. *Inorg. Chem.* **1993**, *32*, 3528–3531.

(99) Lever, A. B. P. Electrochemical parametrization of metal complex redox potentials, using the ruthenium(III)/ruthenium(II) couple to generate a ligand electrochemical series. *Inorg. Chem.* **1990**, *29*, 1271–1285.

(100) Grimme, S.; Hansen, A.; Ehlert, S.; Mewes, J.-M. $r^2$SCAN-3c: A "Swiss army knife" composite electronic-structure method. *J. Chem. Phys.* **2021**, *154*, 064103.

(101) TURBOMOLE V7.5.1 2021, a development of University of Karlsruhe and Forschungszentrum Karlsruhe GmbH, 1989-2007, TURBOMOLE GmbH, since 2007; available from
`https://www.turbomole.org`.

(102) Balasubramani, S. G.; Chen, G. P.; Coriani, S.; Diedenhofen, M.; Frank, M. S.; Franzke, Y. J.; Furche, F.; Grotjahn, R.; Harding, M. E.; Hättig, C.; Hellweg, A.;

Helmich-Paris, B.; Holzer, C.; Huniar, U.; Kaupp, M.; Marefat Khah, A.; Karbalaei Khani, S.; Müller, T.; Mack, F.; Nguyen, B. D.; Parker, S. M.; Perlt, E.; Rappoport, D.; Reiter, K.; Roy, S.; Rückert, M.; Schmitz, G.; Sierka, M.; Tapavicza, E.; Tew, D. P.; van Wüllen, C.; Voora, V. K.; Weigend, F.; Wodyński, A.; Yu, J. M. TURBOMOLE: Modular program suite for ab initio quantum-chemical and condensed-matter simulations. *J. Chem. Phys.* **2020**, *152*, 184107.

(103) Weigend, F.; Ahlrichs, R. Balanced basis sets of split valence, triple zeta valence and quadruple zeta valence quality for H to Rn: Design and assessment of accuracy. *Phys. Chem. Chem. Phys.* **2005**, *7*, 3297–3305.

(104) Neese, F. Software update: The ORCA program system—Version 5.0. *WIREs Comput Mol Sci.* **2022**, *12*, e1606.

(105) Perdew, J. P.; Burke, K.; Ernzerhof, M. Generalized Gradient Approximation Made Simple. *Phys. Rev. Lett.* **1996**, *77*, 3865–3868.

(106) Perdew, J. P.; Burke, K.; Ernzerhof, M. Generalized Gradient Approximation Made Simple [Phys. Rev. Lett. 77, 3865 (1996)]. *Phys. Rev. Lett.* **1997**, *78*, 1396–1396.

(107) Furness, J. W.; Kaplan, A. D.; Ning, J.; Perdew, J. P.; Sun, J. Accurate and Numerically Efficient r$^2$SCAN Meta-Generalized Gradient Approximation. *J. Phys. Chem. Lett.* **2020**, *11*, 8208–8215.

(108) Furness, J. W.; Kaplan, A. D.; Ning, J.; Perdew, J. P.; Sun, J. Correction to: 'Accurate and Numerically Efficient r$^2$SCAN Meta-Generalized Gradient Approximation' (J. Phys. Chem. Lett. (2020) 11:19 (8208-8215) DOI: 10.1021/acs.jpclett.0c02405). *J. Phys. Chem. Lett.* **2020**, 9248.

(109) Zhao, Y.; Truhlar, D. G. A new local density functional for main-group thermochemistry, transition metal bonding, thermochemical kinetics, and noncovalent interactions. *J. Chem. Phys.* **2006**, *125*, 194101.

(110) Adamo, C.; Barone, V. Toward reliable density functional methods without adjustable parameters: The PBE0 model. *J. Chem. Phys.* **1999**, *110*, 6158–6170.

(111) Bursch, M.; Neugebauer, H.; Ehlert, S.; Grimme, S. Dispersion corrected r2SCAN based global hybrid functionals: r2SCANh, r2SCAN0, and r2SCAN50. *J. Chem. Phys.* **2022**, *156*, 134105.

(112) Becke, A. D. Density-functional thermochemistry. III. The role of exact exchange. *J. Chem. Phys.* **1993**, *98*, 5648–5652.

(113) Stephens, P. J.; Devlin, F. J.; Chabalowski, C. F.; Frisch, M. J. Ab Initio Calculation of Vibrational Absorption and Circular Dichroism Spectra Using Density Functional Force Fields. *J. Phys. Chem.* **1994**, *98*, 11623–11627.

(114) Zhao, Y.; Truhlar, D. G. Design of density functionals that are broadly accurate for thermochemistry, thermochemical kinetics, and nonbonded interactions. *J. Phys. Chem. A* **2005**, *109*, 5656–5667.

(115) Zhao, Y.; Truhlar, D. G. The M06 suite of density functionals for main group thermochemistry, thermochemical kinetics, noncovalent interactions, excited states, and transition elements: two new functionals and systematic testing of four M06-class functionals and 12 other functionals. *Theor. Chem. Acc.* **2008**, *120*, 215–241.

(116) Mardirossian, N.; Head-Gordon, M. ωB97X-V: A 10-parameter, range-separated hybrid, generalized gradient approximation density functional with nonlocal correlation, designed by a survival-of-the-fittest strategy. *Phys. Chem. Chem. Phys.* **2014**, *16*, 9904–9924.

(117) Goerigk, L.; Grimme, S. Efficient and Accurate Double-Hybrid-Meta-GGA Density Functionals—Evaluation with the Extended GMTKN30 Database for General Main Group Thermochemistry, Kinetics, and Noncovalent Interactions. *J. Chem. Theory Comput.* **2011**, *7*, 291–309, PMID: 26596152.

(118) Helmich-Paris, B. A trust-region augmented Hessian implementation for restricted and unrestricted Hartree–Fock and Kohn–Sham methods. *J. Chem. Phys.* **2021**, *154*, 164104.

(119) Neese, F. An improvement of the resolution of the identity approximation for the formation of the Coulomb matrix. *J. Comput. Chem.* **2003**, *24*, 1740–1747.

(120) Weigend, F. Accurate Coulomb-fitting basis sets for H to Rn. *Phys. Chem. Chem. Phys.* **2006**, *8*, 1057–1065.

(121) Neese, F.; Wennmohs, F.; Hansen, A.; Becker, U. Efficient, approximate and parallel Hartree–Fock and hybrid DFT calculations. A 'chain-of-spheres' algorithm for the Hartree–Fock exchange. *Chem. Phys.* **2009**, *356*, 98–109.

(122) Izsák, R.; Neese, F. An overlap fitted chain of spheres exchange method. *J. Chem. Phys.* **2011**, *135*, 144105.

(123) Helmich-Paris, B.; de Souza, B.; Neese, F.; Izsák, R. An improved chain of spheres for exchange algorithm. *J. Chem. Phys.* **2021**, *155*, 104109.

(124) Caldeweyher, E.; Ehlert, S.; Hansen, A.; Neugebauer, H.; Spicher, S.; Bannwarth, C.; Grimme, S. A generally applicable atomic-charge dependent London dispersion correction. *J. Chem. Phys.* **2019**, *150*, 154122.

(125) Generally Applicable Atomic-Charge Dependent London Dispersion Correction (https://github.com/dftd4/dftd4).

(126) Haasler, M.; Maier, T. M.; Grotjahn, R.; Gückel, S.; Arbuznikov, A. V.; Kaupp, M. A Local Hybrid Functional with Wide Applicability and Good Balance between (De)Localization and Left–Right Correlation. *J. Chem. Theory Comput.* **2020**, *16*, 5645–5657, PMID: 32697913.

(127) Kong, J.; Proynov, E. Density Functional Model for Nondynamic and Strong Correlation. *J. Chem. Theory Comput.* **2016**, *12*, 133–143, PMID: 26636190.

(128) The xTron code has been developed by Jing Kong's group at Middle Tennessee State University and is available on Github https://github.com/jingkongmtsu/xTron.mKP16.

(129) Epifanovsky, E.; Gilbert, A. T. B.; Feng, X.; Lee, J.; Mao, Y.; Mardirossian, N.; Pokhilko, P.; White, A. F.; Coons, M. P.; Dempwolff, A. L.; Gan, Z.; Hait, D.; Horn, P. R.; Jacobson, L. D.; Kaliman, I.; Kussmann, J.; Lange, A. W.; Lao, K. U.; Levine, D. S.; Liu, J.; McKenzie, S. C.; Morrison, A. F.; Nanda, K. D.; Plasser, F.; Rehn, D. R.; Vidal, M. L.; You, Z.-Q.; Zhu, Y.; Alam, B.; Albrecht, B. J.; Aldossary, A.; Alguire, E.; Andersen, J. H.; Athavale, V.; Barton, D.; Begam, K.; Behn, A.; Bellonzi, N.; Bernard, Y. A.; Berquist, E. J.; Burton, H. G. A.; Carreras, A.; Carter-Fenk, K.; Chakraborty, R.; Chien, A. D.; Closser, K. D.; Cofer-Shabica, V.; Dasgupta, S.; de Wergifosse, M.; Deng, J.; Diedenhofen, M.; Do, H.; Ehlert, S.; Fang, P.-T.; Fatehi, S.; Feng, Q.; Friedhoff, T.; Gayvert, J.; Ge, Q.; Gidofalvi, G.; Goldey, M.; Gomes, J.; González-Espinoza, C. E.; Gulania, S.; Gunina, A. O.; Hanson-Heine, M. W. D.; Harbach, P. H. P.; Hauser, A.; Herbst, M. F.; Hernández Vera, M.; Hodecker, M.; Holden, Z. C.; Houck, S.; Huang, X.; Hui, K.; Huynh, B. C.; Ivanov, M.; Jász, A.; Ji, H.; Jiang, H.; Kaduk, B.; Kähler, S.; Khistyaev, K.; Kim, J.; Kis, G.; Klunzinger, P.; Koczor-Benda, Z.; Koh, J. H.; Kosenkov, D.; Koulias, L.; Kowalczyk, T.; Krauter, C. M.; Kue, K.; Kunitsa, A.; Kus, T.; Ladjánszki, I.; Landau, A.; Lawler, K. V.; Lefrancois, D.; Lehtola, S.; Li, R. R.; Li, Y.-P.; Liang, J.; Liebenthal, M.; Lin, H.-H.; Lin, Y.-S.; Liu, F.; Liu, K.-Y.; Loipersberger, M.; Luenser, A.; Manjanath, A.; Manohar, P.; Mansoor, E.; Manzer, S. F.; Mao, S.-P.; Marenich, A. V.; Markovich, T.; Mason, S.; Maurer, S. A.; McLaughlin, P. F.; Menger, M. F. S. J.; Mewes, J.-M.; Mewes, S. A.; Morgante, P.; Mullinax, J. W.;

Oosterbaan, K. J.; Paran, G.; Paul, A. C.; Paul, S. K.; Pavošević, F.; Pei, Z.; Prager, S.; Proynov, E. I.; Rák, A.; Ramos-Cordoba, E.; Rana, B.; Rask, A. E.; Rettig, A.; Richard, R. M.; Rob, F.; Rossomme, E.; Scheele, T.; Scheurer, M.; Schneider, M.; Sergueev, N.; Sharada, S. M.; Skomorowski, W.; Small, D. W.; Stein, C. J.; Su, Y.-C.; Sundstrom, E. J.; Tao, Z.; Thirman, J.; Tornai, G. J.; Tsuchimochi, T.; Tubman, N. M.; Veccham, S. P.; Vydrov, O.; Wenzel, J.; Witte, J.; Yamada, A.; Yao, K.; Yeganeh, S.; Yost, S. R.; Zech, A.; Zhang, I. Y.; Zhang, X.; Zhang, Y.; Zuev, D.; Aspuru-Guzik, A.; Bell, A. T.; Besley, N. A.; Bravaya, K. B.; Brooks, B. R.; Casanova, D.; Chai, J.-D.; Coriani, S.; Cramer, C. J.; Cserey, G.; DePrince, I., A. Eugene; DiStasio, J., Robert A.; Dreuw, A.; Dunietz, B. D.; Furlani, T. R.; Goddard, I., William A.; Hammes-Schiffer, S.; Head-Gordon, T.; Hehre, W. J.; Hsu, C.-P.; Jagau, T.-C.; Jung, Y.; Klamt, A.; Kong, J.; Lambrecht, D. S.; Liang, W.; Mayhall, N. J.; McCurdy, C. W.; Neaton, J. B.; Ochsenfeld, C.; Parkhill, J. A.; Peverati, R.; Rassolov, V. A.; Shao, Y.; Slipchenko, L. V.; Stauch, T.; Steele, R. P.; Subotnik, J. E.; Thom, A. J. W.; Tkatchenko, A.; Truhlar, D. G.; Van Voorhis, T.; Wesolowski, T. A.; Whaley, K. B.; Woodcock, I., H. Lee; Zimmerman, P. M.; Faraji, S.; Gill, P. M. W.; Head-Gordon, M.; Herbert, J. M.; Krylov, A. I. Software for the frontiers of quantum chemistry: An overview of developments in the Q-Chem 5 package. *J. Chem. Phys.* **2021**, *155*, 084801.

(130) VOORHIS, T. V.; HEAD-GORDON, M. A geometric approach to direct minimization. *Mol. Phys.* **2002**, *100*, 1713–1721.

(131) Gill, P. M.; Johnson, B. G.; Pople, J. A. A standard grid for density functional calculations. *Chem. Phys. Lett.* **1993**, *209*, 506–512.

(132) Li Manni, G.; Kats, D.; Tew, D. P.; Alavi, A. Role of Valence and Semicore Electron Correlation on Spin Gaps in Fe(II)-Porphyrins. *J. Chem. Theory Comput.* **2019**, *15*, 1492–1497, PMID: 30681852.

(133) Piecuch, P.; Wloch, M. Renormalized coupled-cluster methods exploiting left eigenstates of the similarity-transformed Hamiltonian. *J. Chem. Phys.* **2005**, *123*.

(134) Wloch, M.; Gour, J. R.; Piecuch, P. Extension of the Renormalized Coupled-Cluster Methods Exploiting Left Eigenstates of the Similarity-Transformed Hamiltonian to Open-Shell Systems: A Benchmark Study. *J. Phys. Chem. A* **2007**, *111*, 11359–11382.

(135) Barca, G. M. J.; Bertoni, C.; Carrington, L.; Datta, D.; De Silva, N.; Deustua, J. E.; Fedorov, D. G.; Gour, J. R.; Gunina, A. O.; Guidez, E.; Harville, T.; Irle, S.; Ivanic, J.; Kowalski, K.; Leang, S. S.; Li, H.; Li, W.; Lutz, J. J.; Magoulas, I.; Mato, J.; Mironov, V.; Nakata, H.; Pham, B. Q.; Piecuch, P.; Poole, D.; Pruitt, S. R.; Rendell, A. P.; Roskop, L. B.; Ruedenberg, K.; Sattasathuchana, T.; Schmidt, M. W.; Shen, J.; Slipchenko, L.; Sosonkina, M.; Sundriyal, V.; Tiwari, A.; Galvez Vallejo, J. L.; Westheimer, B.; Wloch, M.; Xu, P.; Zahariev, F.; Gordon, M. S. Recent developments in the general atomic and molecular electronic structure system. *J. Chem. Phys.* **2020**, *152*, 154102.

(136) A performant parallel implementation is available in GAMESS, according to the developers, but this did not run on the hardware available to us, which significantly limited the application of the CR-CC(2,3) method.

(137) Sharma, S.; Holmes, A. A.; Jeanmairet, G.; Alavi, A.; Umrigar, C. J. Semistochastic Heat-Bath Configuration Interaction Method: Selected Configuration Interaction with Semistochastic Perturbation Theory. *J. Chem. Theory Comput.* **2017**, *13*, 1595–1604, PMID: 28263594.

(138) Smith, J. E. T.; Mussard, B.; Holmes, A. A.; Sharma, S. Cheap and Near Exact CASSCF with Large Active Spaces. *J. Chem. Theory Comput.* **2017**, *13*, 5468–5478, PMID: 28968097.

(139) Sun, Q.; Zhang, X.; Banerjee, S.; Bao, P.; Barbry, M.; Blunt, N. S.; Bogdanov, N. A.;

Booth, G. H.; Chen, J.; Cui, Z.-H.; Eriksen, J. J.; Gao, Y.; Guo, S.; Hermann, J.; Hermes, M. R.; Koh, K.; Koval, P.; Lehtola, S.; Li, Z.; Liu, J.; Mardirossian, N.; McClain, J. D.; Motta, M.; Mussard, B.; Pham, H. Q.; Pulkin, A.; Purwanto, W.; Robinson, P. J.; Ronca, E.; Sayfutyarova, E. R.; Scheurer, M.; Schurkus, H. F.; Smith, J. E. T.; Sun, C.; Sun, S.-N.; Upadhyay, S.; Wagner, L. K.; Wang, X.; White, A.; Whitfield, J. D.; Williamson, M. J.; Wouters, S.; Yang, J.; Yu, J. M.; Zhu, T.; Berkelbach, T. C.; Sharma, S.; Sokolov, A. Y.; Chan, G. K.-L. Recent developments in the PySCF program package. *J. Chem. Phys.* **2020**, *153*, 024109.

(140) R Core Team, R: A Language and Environment for Statistical Computing. R Foundation for Statistical Computing: Vienna, Austria, 2022.

(141) Lee, J.; Head-Gordon, M. Distinguishing artificial and essential symmetry breaking in a single determinant: approach and application to the C60, C36, and C20 fullerenes. *Phys. Chem. Chem. Phys.* **2019**, *21*, 4763–4778.

(142) Grimme, S.; Hansen, A. A Practicable Real-Space Measure and Visualization of Static Electron-Correlation Effects. *Angew. Chem. Int. Ed.* **2015**, *54*, 12308–12313.

(143) Ramos-Cordoba, E.; Salvador, P.; Matito, E. Separation of dynamic and nondynamic correlation. *Phys. Chem. Chem. Phys.* **2016**, *18*, 24015–24023.

(144) Ramos-Cordoba, E.; Matito, E. Local Descriptors of Dynamic and Nondynamic Correlation. *J. Chem. Theory Comput.* **2017**, *13*, 2705–2711, PMID: 28520420.

(145) Kesharwani, M. K.; Sylvetsky, N.; Köhn, A.; Tew, D. P.; Martin, J. M. L. Do CCSD and approximate CCSD-F12 variants converge to the same basis set limits? The case of atomization energies. *J. Chem. Phys.* **2018**, *149*, 154109.

(146) Lee, T. J.; Taylor, P. R. A diagnostic for determining the quality of single-reference electron correlation methods. *Int. J. Quantum Chem.* **1989**, *36*, 199–207.

(147) Cadima, J.; Cerdeira, J.; Minhoto, M. Computational aspects of algorithms for variable selection in the context of principal components. *Comput. Stat. Data. Anal.* **2004**, *47*, 225–236, Applications of Optimization Heuristics to Estimation and Modelling Problems.

(148) Yuan, H.; Cremer, D. The expectation value of the spin operator $\hat{S}^2$ as a diagnostic tool in coupled cluster theory: The advantages of using UHF-CCSD theory for the description of homolytic dissociation. *Chem. Phys. Lett.* **2000**, *324*, 389–402.

(149) Shee, J.; Arthur, E. J.; Zhang, S.; Reichman, D. R.; Friesner, R. A. Singlet–triplet energy gaps of organic biradicals and polyacenes with auxiliary-field quantum Monte Carlo. *J. Chem. Theory Comput.* **2019**, *15*, 4924–4932.

(150) Yamaguchi, K.; Jensen, F.; Dorigo, A.; Houk, K. A spin correction procedure for unrestricted Hartree-Fock and Møller-Plesset wavefunctions for singlet diradicals and polyradicals. *Chem. Phys. Lett.* **1988**, *149*, 537–542.

(151) Saito, T.; Yasuda, N.; Kataoka, Y.; Nakanishi, Y.; Kitagawa, Y.; Kawakami, T.; Yamanaka, S.; Okumura, M.; Yamaguchi, K. Potential Energy Curve for Ring-Opening Reactions: Comparison Between Broken-Symmetry and Multireference Coupled Cluster Methods. *J. Phys. Chem. A* **2011**, *115*, 5625–5631, PMID: 21568304.

(152) Margraf, J. T.; Perera, A.; Lutz, J. J.; Bartlett, R. J. Single-reference coupled cluster theory for multi-reference problems. *J. Chem. Phys.* **2017**, *147*, 184101.

(153) Schurkus, H.; Chen, D.-T.; Cheng, H.-P.; Chan, G.; Stanton, J. Theoretical prediction of magnetic exchange coupling constants from broken-symmetry coupled cluster calculations. *J. Chem. Phys.* **2020**, *152*, 234115.

(154) Wodyński, A.; Kaupp, M. Local Hybrid Functional Applicable to Weakly and Strongly Correlated Systems. *J. Chem. Theory Comput.* **2022**, *18*, 6111–6123, PMID: 36170626.

(155) Santra, G.; Martin, J. M. L. Do Double-Hybrid Functionals Benefit from Regularization in the PT2 Term? Observations from an Extensive Benchmark. *J. Phys. Chem. Lett.* **2022**, *13*, 3499–3506, PMID: 35417181.

(156) Ma, Q.; Werner, H.-J. Explicitly correlated local coupled-cluster methods using pair natural orbitals. *Wiley Interdiscip. Rev. Comput. Mol. Sci.* **2018**, *8*, e1371.

# TOC Graphic

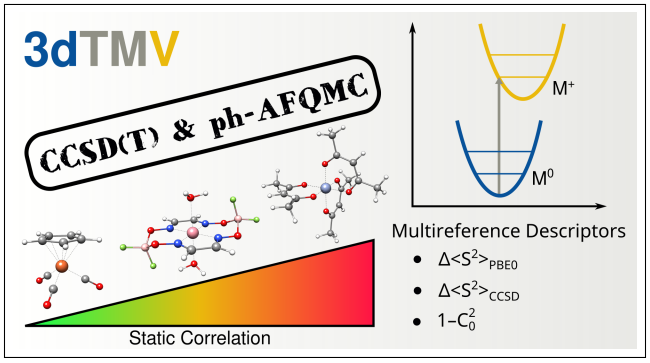
3dTMV
CCSD(T) & ph-AFQMC
Static Correlation
M+
M0
Multireference Descriptors
Δ<S2>PBE0
Δ<S2>CCSD
1−C02